

Reaction dynamics of carbon-bearing radicals in circumstellar envelopes of carbon stars

Xibin Gu,^a Ying Guo,^a Fangtong Zhang,^a Alexander M. Mebel^b and Ralf I. Kaiser^{*a}

Received 22nd November 2005, Accepted 30th January 2006

First published as an Advance Article on the web 19th May 2006

DOI: 10.1039/b516457e

Crossed molecular beams experiments on dicarbon molecules, $C_2(X^1\Sigma_g^+/a^3\Pi_u)$, with unsaturated hydrocarbons acetylene ($C_2H_2(X^1\Sigma_g^+)$), ethylene ($C_2H_4(X^1A_g)$), methylacetylene ($CH_3CCH(X^1A_1)$), and allene ($H_2CCCH_2(X^1A_1)$) were carried out at 18 collision energies between 10.6 and 50.3 kJ mol⁻¹ utilizing a universal crossed beams machine to untangle the reaction dynamics forming hydrogen deficient hydrocarbon radicals in circumstellar envelopes of carbon stars and in cold molecular clouds. We find that all reactions proceed without the entrance barrier through indirect (complex forming) scattering dynamics. Each bimolecular collision is initiated by an addition of the dicarbon molecule to the π bond of the unsaturated hydrocarbon molecule yielding initially acyclic (triplet) and three- or four-membered cyclic collision complexes (triplet and singlet surface). On the singlet surface, the cyclic structures isomerize to form eventually diacetylene ($HCCCCH$; C_2/C_2H_2), butatriene ($H_2CCCCCH_2$; C_2/C_2H_4), methyldiacetylene (CH_3CCCCH ; C_2/CH_3CCH), and pentatetraene ($H_2CCCCCH_2$; C_2/H_2CCCH_2) intermediates. The latter were found to decompose *via* atomic hydrogen loss yielding the buta-1,3-diyanyl [$C_4H(X^2\Sigma^+) HCCCC$], 1-butene-3-yne-2-yl [$i-C_4H_3(X^2A') H_2CCCCH$], penta-2,4-diyanyl-1 [$C_5H_3(X^2B_1) HCCCCCH_2$], and penta-1,4-diyanyl-3 radical [$C_5H_3(X^2B_1) HCCCCHCCH$] under single collision conditions. The underlying characteristics of these dicarbon *versus* atomic hydrogen replacement pathways (indirect scattering dynamics; no entrance barrier; isomerization barriers below the energy of the separated reactants; exoergic reactions) suggest the enormous potential of the dicarbon plus unsaturated hydrocarbon reaction class to form highly hydrogen-deficient carbonaceous molecules in cold molecular clouds and in circumstellar envelopes of carbon stars. The studies therefore present an important advancement in establishing a comprehensive database of reaction intermediates and products involved in bimolecular collisions of dicarbon molecules with unsaturated hydrocarbons which can be utilized in refined astrochemical models and also in future searches of hitherto unidentified interstellar molecules. Implications of these experiments to understand related combustion processes are also addressed.

1. Introduction

The reaction dynamics and energetics of the bare carbon clusters $C_2(X^1\Sigma_g^+)$ (dicarbon) and $C_3(X^1\Sigma_g^+)$ (tricarbon) with unsaturated hydrocarbons are of paramount importance in understanding combustion processes^{1,2} and the chemical evolution of extraterrestrial environments such as molecular clouds and circumstellar envelopes of dying carbon stars, for instance, IRC + 10216.³ Reactions of the dicarbon molecule in its $X^1\Sigma_g^+$ electronic ground and first electronically excited $a^3\Pi_u$ state are of particular pertinence in untangling the formation of polycyclic aromatic

^a Department of Chemistry, University of Hawaii at Manoa, Honolulu HI 96822, USA

^b Department of Chemistry and Biochemistry, Florida International University, Miami FL 33199, USA

hydrocarbons (PAHs), their hydrogen deficient precursors, and of carbon-rich nanostructures up to fullerenes from the ‘bottom up’.⁴ In the interstellar medium, these sub-micrometer sized carbonaceous nanoparticles are thought to be primarily composed of nanometer-sized stacks of planar layers of carbon atoms. Those layers can be characterized as fused benzene rings and are likely formed *via* agglomeration of polycyclic aromatic hydrocarbons.^{5,6} Formed primarily as interstellar grains in the outflow of dying carbon stars, they shield polyatomic molecules in dense clouds from the destructive ultraviolet field.⁷ Due to the low temperatures of the grain particles of 10–15 K, these nanoparticles can also act as natural cold traps. Once a molecule or atom from the gas phase collides with the grain nuclei, it can stick to the surface with almost unit efficiency; atomic and molecular hydrogen as well as helium have sticking coefficients below one. This process accumulates icy structures of a few tens of nanometers thick which can act as catalysts to synthesize molecular hydrogen and saturated hydrides like water, ammonia, and methane.⁸ These ices are also processed chemically by photons and cosmic ray particles to form astrobiologically important molecules, such as glycolaldehyde together with the structural isomers acetic acid and methyl formate and possibly amino acids.⁹ Upon star formation, these molecules can be released into the gas phase *via* sublimation¹⁰ and are thought to actively participate in the astrobiological evolution of the interstellar medium.¹¹ The crucial role of nanodiamonds in interstellar space and in chemical vapor deposition on the industrial scale should also be noted.¹²

But despite the key role of carbonaceous nanostructures together with their hydrogen-deficient precursors in the chemical evolution of cold molecular clouds and circumstellar envelopes of carbon stars, the fundamental question ‘How are these nanoparticles and their precursors actually formed?’ has not been resolved conclusively. The majority of mechanistic information on the growth of polycyclic aromatic hydrocarbons and their precursors has been derived from chemical reaction networks which actually model the formation of PAH-like structures in the interstellar medium;³ note that these processes are thought to be similar—with the exception that oxygen is present—to form PAH-like structures in sooting combustion flames.^{1,5} All models suggest that the synthesis of small carbon-bearing radicals is linked to the formation of PAHs and ultimately to the production of carbonaceous nanostructures. Various mechanisms have been postulated; those currently in favour are thought to involve a successive build-up of hydrogen-deficient carbon bearing radicals *via* sequential addition steps of ground state atomic carbon, $C(^3P_j)$, dicarbon and tricarbon clusters (C_2 , C_3), small hydrocarbon radicals (C_2H , C_2H_3 , $1/e-C_3H$, $1/e-C_3H_2$, C_3H_3 , C_3H_5 , $1/n-C_4H_3$, $1/c-C_5H_5$, C_6H_5), and reactions *via* acetylene (C_2H_2), diacetylene (C_4H_2), benzene (C_6H_6), PAH-like structures, and fullerenes.¹³ Note that those species in italics together with SiC, SiC₄, c-SiC₂, and c-SiC₃—precursors to silicon–carbon nanostructures—have actually been observed in the interstellar medium.¹⁴

However, during the last decade the chemical accuracy of these models has come under harsh scrutiny, as the majority of the incorporated reactions have not been comprehensively investigated in laboratory experiments. To assess the role of these neutral–neutral reactions and to include them in the pertinent chemical models of cold molecular clouds and of circumstellar environments, four sets of data are crucial to obtain a legitimate and realistic picture of the formation of carbonaceous nanostructures and their precursors in the interstellar medium. These are (i) rate constants, (ii) the identification of the reaction product(s) and their branching ratios, (iii) an assignment of reaction intermediate(s), and (iv) information on the reaction energies.^{8,15} For instance, a novel study on the hydrocarbon chemistry in solar system environments (here: Neptune’s stratosphere) clearly demonstrates the necessity of these laboratory studies.¹⁶ A thorough error analysis of the input data exposed substantial shortcomings of currently existing models. C_2 compounds like dicarbon, the ethynyl radical, and acetylene were found to be ‘reproduced’ only within error limits of 100%. The data are inflicted with larger uncertainties considering species with three carbon atoms, and errors of 200% were derived. Inaccuracies of 2000% for more complex molecules expose the severe limitations of current reaction networks. The decadal study of the National Aeronautics and Space Administration also recognized the importance of studying these important sets of neutral–neutral reactions.¹⁷ Specifically, the reactions of dicarbon molecules and the formation of resonantly stabilized free radicals (RSFR) were requested to be studied to gain, once and for all, a detailed understanding on the underlying growth processes of PAHs, carbon-rich nanostructures, and their precursors.

Due to this importance, the kinetics of dicarbon reactions have been extensively investigated at room temperature¹⁸ (recall that the electronically excited triplet state, $a^3\Pi_u$, lies only 718.32 cm^{-1} above the ground state $X^1\Sigma_g^+$). In these studies, the disappearance of dicarbon in the two electronic states ($X^1\Sigma_g^+$ and $a^3\Pi_u$) was followed; the reactions of $C_2(X^1\Sigma_g^+)$ were found to be quite fast (of the gas kinetic order when the molecular partner is an unsaturated hydrocarbon) whereas the $C_2(a^3\Pi_u)$ reactions were suggested to be systematically slower. However, despite these extensive kinetic studies, information on the products of dicarbon reactions together with the intermediates involved is still lacking. In some cases, primary products and reaction mechanisms were speculated on the basis of the observed temperature dependence of the reactions. For instance, from the measured removal rate constants of $C_2(X^1\Sigma_g^+)$ and $C_2(a^3\Pi_u)$ by ethylene, the favored approach was suggested to be an addition of the electrophilic C_2 (both singlet and triplet states) to the olefinic π bond. Nevertheless, $C_2(X^1\Sigma_g^+)$ reacts faster than $C_2(a^3\Pi_u)$. This implies that $C_2(X^1\Sigma_g^+)$ could also react through alternative pathways. A few reactions of dicarbon were also investigated at 10 K and 77 K in the condensed phase and *via ab initio* calculations in order to understand the reaction mechanism.¹⁹ Interestingly, the reaction products of the reaction of dicarbon with ethylene have always been speculated to be C_2H and C_2H_3 ($\Delta_r G = -36.7\text{ kJ mol}^{-1}$) or C_2H_2 and C_2H_2 ($\Delta_r G = -435.8\text{ kJ mol}^{-1}$)—so far without any experimental confirmation. These considerations make it exceptionally clear that novel laboratory studies on reactions of dicarbon with unsaturated hydrocarbons which provide reaction products, their branching ratios, the intermediates involved, and the thermodynamic properties of product isomers—data which kinetic measurements can never supply—are clearly imperative.

In this *Faraday Discussion* paper, we focus on the collision-energy dependent reaction dynamics of dicarbon molecules with unsaturated hydrocarbons acetylene ($C_2H_2(X^1\Sigma_g^+)$), ethylene ($C_2H_4(X^1A_g)$), methylacetylene ($CH_3CCH(X^1A_1)$), and allene ($H_2CCCH_2(X^1A_1)$). These systems represent prototype reactions of ubiquitous interstellar dicarbon molecules with hydrocarbons to synthesize hydrocarbon radicals *via* a single neutral–neutral collision in the outflow of carbon rich AGB stars and in cold molecular clouds. Specifically, the closed shell hydrocarbon molecules serve as model reactants with triple (acetylene) and double (ethylene) bonds; methylacetylene and allene are chosen as the simplest representatives of closed shell hydrocarbon species to investigate how the chemical reaction dynamics change from one structural isomer to the other. Transitions of $C_2(X^1\Sigma_g^+)$ were observed, for instance, towards warm carbon stars like IRC + 10126,²⁰ post AGB stars such as HD 56126,²¹ and in the direction of the HII region W40 IRS. Since all chemical processes in cold molecular clouds and circumstellar envelopes consist of multiple elementary reactions that are a series of bimolecular encounters, for instance, between dicarbon molecules and hydrocarbons, a detailed knowledge of the elementary processes involved at the most fundamental, microscopic level under single collision conditions is truly imperative. This means that in a bimolecular reaction of a dicarbon molecule with an unsaturated hydrocarbon, one carbon cluster reacts with only one hydrocarbon molecule without collisional stabilization and/or successive reaction of the potential reaction intermediate(s). The primary reaction products are expected to be highly hydrogen deficient carbon bearing molecules; their spectroscopic properties are often unknown. Therefore, these products are difficult to monitor by optical detection methods, and a ‘universal’ detector is crucial in experiments when the nature itself of the product is obscure.

The crossed molecular beam technique with mass spectrometric detection has been established as a powerful technique to achieve these requirements and to observe radical product formation under well-characterized experimental conditions in the gas phase. In contrast to bulk experiments, where reactants are mixed, the main advantage of a crossed beams approach is the capability to form the reactants in separate, supersonic beams. In principle, both reactant beams can be prepared in well-defined quantum states before they cross at a specific collision energy under single collision conditions. Since investigations are performed at the molecular, microscopic level in a collision free environment—where it is possible to observe the consequences of a single reactive event—this approach provides a complete insight into the reaction mechanism as the nature of the primary reaction products can be inferred. When the products are polyatomic molecules, the crossed beam technique with mass spectrometric detection has proved to be essential in identifying the relevant reaction pathways.²² In fact, when distinct structural isomers—molecules with the same chemical formula but different arrangements of atoms—might be formed, knowledge of chemical reaction dynamics is crucial in order to assign the isomer(s) produced.

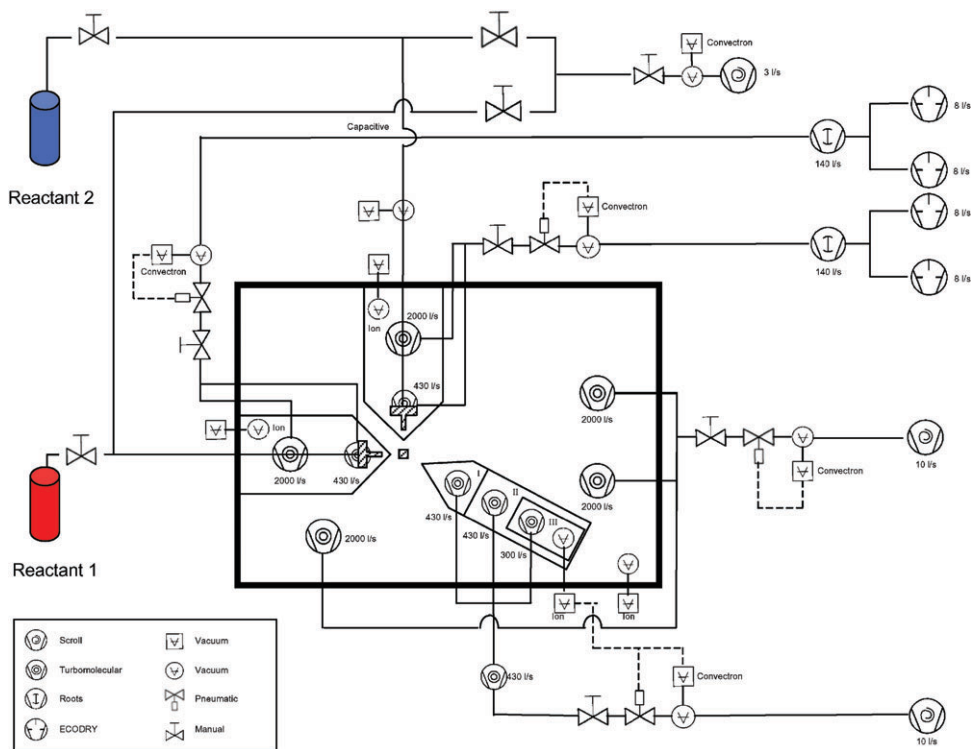


Fig. 1 Pumping and interlock scheme of the crossed molecular beams machine.

2. Experimental setup

2.1. The main chamber

The reactive scattering experiments were carried out under single collision conditions in a crossed molecular beams machine at The University of Hawaii.²³ Briefly, the main chamber consists of a 304 stainless steel box (180 cm × 160 cm × 80 cm; 2300 l) and is pumped by three 2000 l s⁻¹ magnetically suspended turbo molecular pumps (Osaka Vacuum; TG2003) backed by one scroll pump (Edwards XD35; 10 l s⁻¹) to the low 10⁻⁸ Torr region (Fig. 1 and 2). To reduce the background from straight-through molecules into the detector, the machine is equipped with a cold shield located between the chopper wheel and the interaction region (primary source) and downstream the skimmer (secondary source). The oxygen free high conductivity (OFHC) copper shield is interfaced to the second stage (10 K) of a CTI CP-1020 cold head and reduces the vacuum in the main chamber to 4 × 10⁻⁹ Torr. This arrangement limits the pressure in the main chamber during a crossed beams experiment to the low to medium 10⁻⁷ Torr regime. Both source chambers are located inside the main chamber so that the reactant beams cross perpendicularly. Each source chamber is evacuated by a 2000 l s⁻¹ and a 430 l s⁻¹ maglev pump (Osaka Vacuum; TG2003 and TG430) to the medium 10⁻⁹ Torr region; operating pulsed sources increase the pressure to about 10⁻⁵ Torr. A dry roots pump (Leybold WS505; 140 l s⁻¹) roughed by two oil-free EcoDry M30 pumps (Leybold; 16 l s⁻¹) backs the turbo pumps of each source chamber. The schematic top view of the machine is shown in Fig. 3.

2.2. Preparation of supersonic reactant beams

The generation of supersonic reactant beams of sufficiently high concentration to guarantee a detectable quantity of the final reaction product(s) is essential. In our experiments, the 30 Hz output of a Spectra Physics GCR 270-30 Nd-YAG was focused onto a rotating carbon rod.²⁴ The ablated

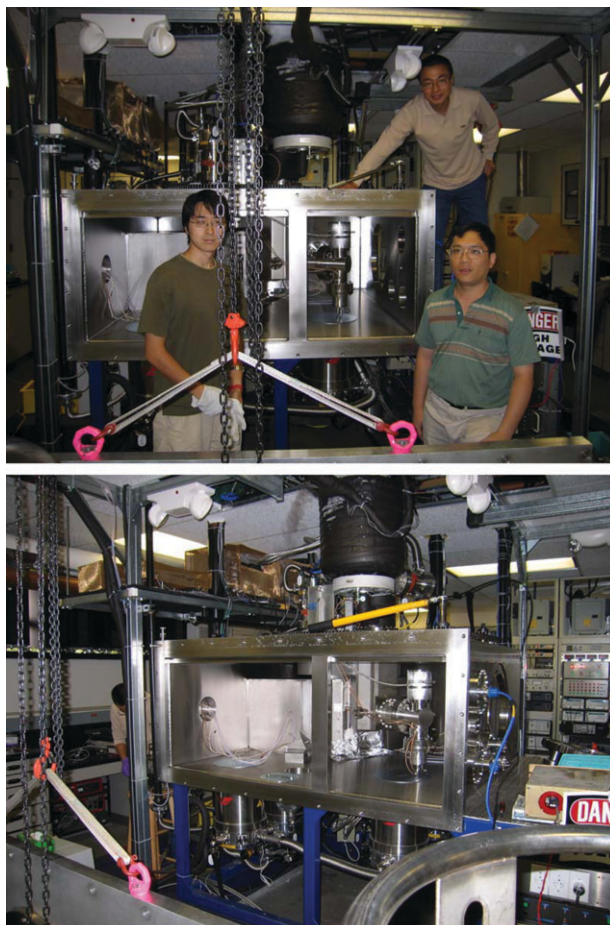


Fig. 2 Images of the crossed molecular beams machine.

species (atomic carbon $C(^3P)$), dicarbon $C_2(X^1\Sigma_g^+/a^3\Pi_u)$, tricarbon $C_3(X^1\Sigma_g^+)$) were seeded in neat carrier gas (helium, 99.9999%; neon, 99.9999%; argon: 99.9999%) released by a Proch–Trickl pulsed valve (1.0 mm nozzle diameter). The latter was operated at -400 V with 60 Hz, 80 μ s pulses, and 4 atm backing pressure. Typically, the ablation laser was fired 150–165 μ s after the pulsed valve has been triggered; this time sequence maximizes the number density of the dicarbon molecules in the interaction region to about 3×10^{13} cm^{-3} . The seeded beam passed the skimmer of 1.0 mm diameter. Most importantly, in the case of laser-based ablation sources,^{25,26} the chemical composition of the supersonic beam and the peak velocity differ in distinct segments of the pulsed beam. For instance, electronically and/or vibrationally excited species may prevail in the predominantly faster and hence less cooled parts of the beam. Therefore, to select a reactant beam of a well defined chemical composition and velocity distribution, fast rotating chopper wheels are often utilized.²⁷ Here, a four-slot chopper wheel mounted after the ablation zone selected a segment of the pulse (Table 1). This segment of the dicarbon beam, which contained dicarbon in its $X^1\Sigma_g^+$ electronic ground state as well as in its first electronically excited $a^3\Pi_u$ state—crossed a pulsed hydrocarbon beam (acetylene, ethylene, allene, or methylacetylene) released by a second pulsed valve perpendicularly under a well-defined collision energy in the interaction region (-500 V; 80 μ s pulses; 550 Torr backing pressure; 0.75 mm nozzle diameter) (Table 1). Since the dicarbon beam was actually faster than the supersonic hydrocarbon beams, the pulsed valve of the secondary source had to be opened 10–20 μ s prior to the one in the primary source. Although the primary beam

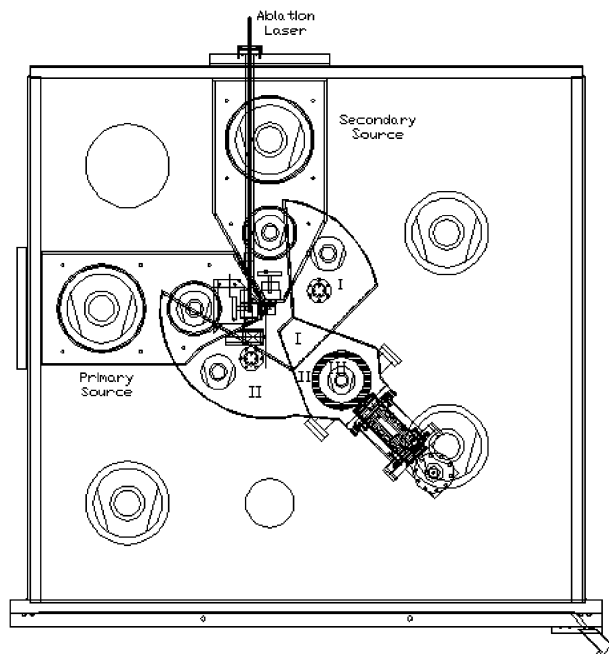


Fig. 3 Top view of the experimental setup with differentially pumped regions I–III, source chambers, chopper wheel, ablation source, and laser channel.

Table 1 Peak velocities (v_p), speed ratios (S), center-of-mass angles (θ_{CM}), together with the nominal collision energies of the dicarbon and hydrocarbon reactants (E_c)

Beam	v_p/ms^{-1}	S	$E_c/\text{kJ mol}^{-1}$	θ_{CM}
$\text{C}_2\text{H}_2(\text{X}^1\Sigma_g^+)$	902 ± 2	16.0 ± 0.3	—	—
$\text{C}_2(\text{X}^1\Sigma_g^+/\text{a}^3\Pi_u)/\text{Ar}$	944 ± 8	5.0 ± 0.1	10.6 ± 0.1	46.0 ± 0.3
$\text{C}_2(\text{X}^1\Sigma_g^+/\text{a}^3\Pi_u)/\text{Ne}$	1060 ± 17	4.7 ± 0.5	12.1 ± 0.2	42.7 ± 0.5
$\text{C}_2(\text{X}^1\Sigma_g^+/\text{a}^3\Pi_u)/\text{He}$	1629 ± 6	5.2 ± 0.1	21.6 ± 0.2	31.0 ± 0.2
$\text{C}_2(\text{X}^1\Sigma_g^+/\text{a}^3\Pi_u)/\text{He}$	1956 ± 23	5.7 ± 0.2	29.0 ± 0.5	26.5 ± 0.2
$\text{C}_2(\text{X}^1\Sigma_g^+/\text{a}^3\Pi_u)/\text{He}$	2362 ± 42	4.9 ± 0.3	39.9 ± 0.2	22.5 ± 0.4
$\text{C}_2(\text{X}^1\Sigma_g^+/\text{a}^3\Pi_u)/\text{He}$	2608 ± 36	4.1 ± 0.2	47.5 ± 1.2	20.5 ± 0.2
$\text{C}_2\text{H}_4(\text{X}^1\text{A}_g)$	893 ± 3	15.7 ± 0.2	—	—
$\text{C}_2(\text{X}^1\Sigma_g^+/\text{a}^3\Pi_u)/\text{Ne}$	1041 ± 9	5.7 ± 0.2	12.1 ± 0.1	44.9 ± 0.3
$\text{C}_2(\text{X}^1\Sigma_g^+/\text{a}^3\Pi_u)/\text{Ne}$	1513 ± 25	3.4 ± 0.1	19.9 ± 0.5	34.5 ± 0.5
$\text{C}_2(\text{X}^1\Sigma_g^+/\text{a}^3\Pi_u)/\text{He}$	1966 ± 22	5.5 ± 0.2	30.1 ± 0.6	27.8 ± 0.3
$\text{C}_2(\text{X}^1\Sigma_g^+/\text{a}^3\Pi_u)/\text{He}$	2353 ± 96	3.6 ± 0.3	40.9 ± 3.0	23.8 ± 0.9
$\text{CH}_3\text{CCH}(\text{X}^1\text{A}_1)$	840 ± 3	12.0 ± 0.2	—	—
$\text{C}_2(\text{X}^1\Sigma_g^+/\text{a}^3\Pi_u)/\text{Ne}$	1070 ± 20	5.5 ± 0.3	13.9 ± 0.3	52.6 ± 0.5
$\text{C}_2(\text{X}^1\Sigma_g^+/\text{a}^3\Pi_u)/\text{Ne}$	1625 ± 20	3.3 ± 0.1	25.1 ± 0.5	40.7 ± 0.4
$\text{C}_2(\text{X}^1\Sigma_g^+/\text{a}^3\Pi_u)/\text{He}$	2076 ± 25	3.9 ± 0.2	37.6 ± 0.8	34.0 ± 0.3
$\text{C}_2(\text{X}^1\Sigma_g^+/\text{a}^3\Pi_u)/\text{He}$	2450 ± 31	3.9 ± 0.2	50.3 ± 1.2	29.7 ± 0.4
$\text{H}_2\text{CCCH}_2(\text{X}^1\text{A}_1)$	840 ± 3	12.1 ± 0.2	—	—
$\text{C}_2(\text{X}^1\Sigma_g^+/\text{a}^3\Pi_u)/\text{Ne}$	1050 ± 6	5.7 ± 0.2	13.6 ± 0.1	53.1 ± 0.2
$\text{C}_2(\text{X}^1\Sigma_g^+/\text{a}^3\Pi_u)/\text{Ne}$	1682 ± 22	3.2 ± 0.1	26.5 ± 0.6	39.8 ± 0.4
$\text{C}_2(\text{X}^1\Sigma_g^+/\text{a}^3\Pi_u)/\text{He}$	2090 ± 38	4.3 ± 0.3	38.1 ± 1.2	33.8 ± 0.5
$\text{C}_2(\text{X}^1\Sigma_g^+/\text{a}^3\Pi_u)/\text{He}$	2426 ± 40	3.9 ± 0.2	49.4 ± 1.5	30.0 ± 0.4

contains tricarbon molecules, the latter were found not to react with the hydrocarbon molecules of the secondary beam, since these bimolecular reactions have characteristic reaction thresholds of up to 85 kJ mol⁻¹.²⁵ Likewise, the carbon atoms do not—in the case of the atomic and molecular hydrogen replacement channels—interfere with the reactive scattering signal of the dicarbon–hydrocarbon reaction due to a mass difference of 12 amu of potential reaction products (Section 3).²⁶

We would like to stress that the crossed beams reactions were carried out with pulsed molecular beams. Compared to continuous supersonic beams, pulsed beams offer certain advantages. Firstly, pumping requirements and hence involved costs can be reduced drastically due to the limited gas load from the pulsed valves. Secondly—if reactive species of one reactant beam are generated *via* pulsed laser ablation or photolysis of helium-seeded precursor molecules—operating the second beam also in a pulsed mode limits the gas consumption and hence costs of the second reactant molecules; this is of particular importance if isotopically labelled species such as deuterated or ¹³C-substituted hydrocarbon gases are utilized; operating continuous beams of, for instance, HCCD, would certainly bankrupt the PI. Thirdly, pulsed beams allow a greater versatility of the reactant species such as dicarbon molecules to be generated. Stable and intense continuous beams of dicarbon molecules have not yet been established. Finally, pulsed beams allow a simple tuning of the collision energy by merely changing the delay times between both intersecting beams (Table 1).

2.3. Detection of the reactively scattered products

The reactively scattered species are monitored using a quadrupole mass spectrometric detector (QMS) (Fig. 3 and 4). The detector is located in a separate, triply differentially pumped ultra high vacuum chamber (10⁻¹¹ Torr) and is rotatable within the plane defined by both beams. Since every rotation in a vacuum system in the pressure, the rotating detector ring is separated from the atmosphere by three Teflon loaded seals. The spaces between these seals are doubly differentially pumped to reduce the pressure from the atmosphere (760 Torr) *via* 10⁻² Torr and 4 × 10⁻⁸ Torr (Teflon sealed regions) to the low to medium 10⁻⁹ Torr in the main chamber. This arrangement ensures no pressure increase in the main chamber even if the detector is being rotated. Differentially pumped detector regions I/II reduce the gas load from the main chamber, whereas region III contains the Brink-type electron impact ionizer²⁸ surrounded by a liquid nitrogen cold shield. The quadrupole mass filter and the Daly-type scintillation particle detector²⁹ are connected to the second region. Here, each ion hits the surface of a high voltage target (-25 kV) and initiates an electron cascade. The latter is accelerated to an aluminium coated (200 nm) organic scintillator BC-418 (Saint Gobain; 391 nm photon emission) whose photon cascade is detected by a convection cooled photomultiplier tube (PMT; Burle 8850; -(1100–1350) V) mounted outside the UHV detector.³⁰ Magnetic shielding of the PMT and the resistor chain enhances the signal by about 15%. Each PMT pulse then passes a discriminator set between 1.5 and 2.0 mV and is amplified. The outgoing TTL pulse is fed into a multi channel scaler (MCS) operated at dwell times between 0.64 μs (on axis beam diagnostics) and 5.12 μs or 10.24 μs (reactive scattering experiments) to record the time of flight of the ion *versus* the intensity at a defined mass-to-charge ratio (*m/z*) (TOF mode). These TOF spectra can be taken at distinct mass-to-charge ratios (*m/z*) and at different laboratory angles. By taking and integrating the TOF spectra at distinct laboratory angles, we can then obtain the laboratory angular distribution, *i.e.* the integrated signal intensity of an ion of distinct *m/z* *versus* the laboratory angle. Note, that each region is pumped by a magnetically levitated turbo molecular pump (region I/II: 400 l s⁻¹; region III: 380 l s⁻¹); all three pumps are backed by a 400 l s⁻¹ turbo molecular pump whose exhaust is connected to an oil free scroll pump (10 l s⁻¹). This pumping scheme reaches down to the low 10⁻¹¹ Torr in region three; lower pressures down to the high 10⁻¹³ Torr regime can be achieved by operating a cold head inside region three (3.8 K; 1.5 W). The background masses are compiled in Table 2. Thorium and iridium bearing species originate from the thoriated iridium filament, copper from the copper leads to the ionizer, iron/nickel/chromium from the heated stainless steel.

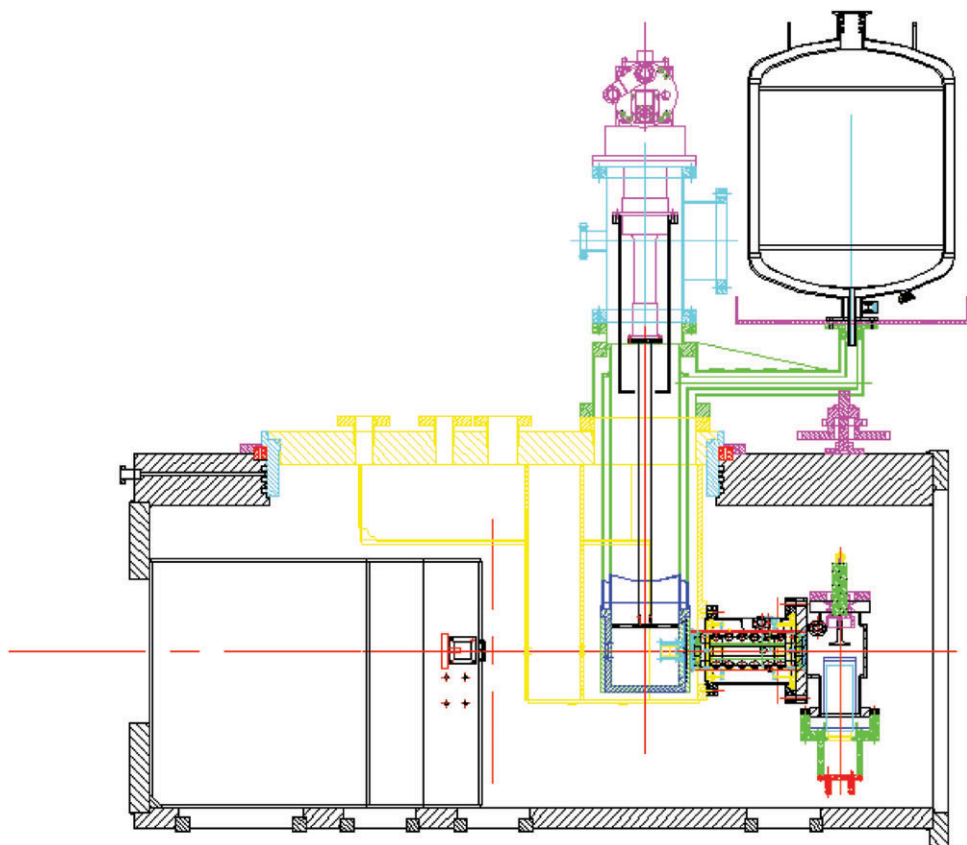


Fig. 4 Side view of the main chamber and of the rotatable detection system of the crossed beams setup with differentially pumped regions I–III, the ionizer (region III), quadrupole rod system (region II), Daly detector (region II), photomultiplier tube (PMT), liquid nitrogen jacket (region III), and cold head (region III).

Table 2 Mass-to-charge (m/z) values and assignment of species observed in the residual gas analyzer mode of our Extrel mass spectrometer at a base pressure of 10^{-11} Torr. Data were taken with the 1.2 MHz oscillator (1–500 amu). Species at m/z values larger than 45 contribute less than 5 counts compared to 3000 counts for $m/z = 28$. Operating the cold head inside the detector eliminates signals at $m/z = 40, 20, 18,$ and 17 (argon, water) and reduces the ion counts at those m/z values in italics. The cold head has no influence on m/z values larger than 45, *i.e.* those species originating from the ionizer filament and the copper/nickel/stainless steel wires

m/z	Assignment	m/z	Assignment	m/z	Assignment	m/z	Assignment
1	$^1\text{H}^+$	17	$^{16}\text{O}^+ / ^{17}\text{O}^+$	50	$^{50}\text{Cr}^+$	64.3	$^{193}\text{Ir}^{3+}$
2	$^1\text{H}_2^+$	18	$^1\text{H}_2^{16}\text{O}^+ / ^{18}\text{O}^+$	52	$^{52}\text{Cr}^+$	65	$^{65}\text{Cu}^+$
3	$^{12}\text{C}^+$	20	$^{40}\text{Ar}^{2+}$	53	$^{53}\text{Cr}^+$	77.3	$^{232}\text{Th}^{3+}$
4	$^{12}\text{C}^{3+}$	28	$^{12}\text{C}^{16}\text{O}^+ / ^{14}\text{N}_2^+ / ^{56}\text{Fe}^{2+}$	54	$^{54}\text{Cr}^+ / ^{54}\text{Fe}^+$	95.5	$^{191}\text{Ir}^{2+}$
6	$^{12}\text{C}^{2+}$	29	$^{13}\text{C}^{16}\text{O}^+ / ^{15}\text{N}^{14}\text{N}^+$	56	$^{56}\text{Fe}^+$	96.5	$^{193}\text{Ir}^{2+}$
7	$^{14}\text{N}^{2+}$	30	$^{12}\text{C}^{18}\text{O}^+$	57	$^{57}\text{Fe}^+$	116	$^{232}\text{Th}^{2+}$
8	$^{16}\text{O}^{2+}$	32	$^{16}\text{O}_2^+$	58	$^{232}\text{Th}^{4+} / ^{58}\text{Ni}^+$	124	$^{232}\text{Th}^{16}\text{O}^{2+}$
12	$^{12}\text{C}^+$	40	$^{40}\text{Ar}^+$	60	$^{60}\text{Ni}^+$	191	$^{191}\text{Ir}^+$
13	$^{13}\text{C}^+ / ^{12}\text{CH}^+$	44	$^{12}\text{C}^{16}\text{O}_2^+$	61	$^{61}\text{Ni}^+$	193	$^{193}\text{Ir}^+$
14	$^{14}\text{N}^+ / ^{12}\text{CH}_2^+$	45	$^{13}\text{C}^{16}\text{O}_2^+$	62	$^{62}\text{Ni}^+$	232	$^{232}\text{Th}^+$
15	$^{15}\text{N}^+ / ^{12}\text{CH}_3^+$	47.8	$^{191}\text{Ir}^{4+}$	63	$^{63}\text{Cu}^+$	248	$^{232}\text{Th}^{16}\text{O}^+$
16	$^{16}\text{O}^+ / ^{12}\text{CH}_4^+$	48.6	$^{193}\text{Ir}^{4+}$	63.7	$^{191}\text{Ir}^{3+}$	264	$^{232}\text{Th}^{16}\text{O}_2^+$

3. Data analysis

For the physical interpretation of the reactive scattering data, it is necessary to transform the laboratory data into the center-of-mass (CM) system.³¹ This enables us to obtain the information on the chemical dynamics of the reaction by fitting the TOF spectra of the reactively scattered products and the product angular distribution in the laboratory frame (LAB) using a forward-convolution routine.³² This procedure initially postulates an angular distribution $T(\theta)$ and a translational energy distribution $P(E_T)$ in the center-of-mass reference frame (CM). Laboratory TOF spectra and the laboratory angular distribution were then calculated from these $T(\theta)$ and $P(E_T)$ accounting for the transformation Jacobian and averaging over the apparatus (chopper frequency; detector opening) and beam functions (velocity spread, angular spread). Best fits of the TOF and laboratory angular distributions were achieved by refining the adjustable $T(\theta)$ parameters and the points of the $P(E_T)$. The final outcome is the generation of a product flux contour map which reports the differential cross section, $I(\theta, u)$, of the product as the intensity as a function of angle θ and product center-of-mass velocity u . This map serves as an image of the reaction and contains all the information of the reactive scattering process.

Also, the dynamics of the dicarbon and carbon atom reactions are quite distinct so that the crossed beams technique—together with the transformation from the laboratory to the center-of-mass frame—allows us to separate the contribution of the dicarbon and carbon reaction. We would like to outline this procedure considering the reaction of atomic carbon and dicarbon with acetylene as an example (Fig. 5).³³ Here, a beam of the dicarbon species with a lab velocity V_{C_2} crosses a beam of acetylene species with a lab velocity $V_{C_2H_2}$ at 90° ; both velocities are represented as velocity vectors. The vector connecting the tips of the dicarbon and acetylene velocity vectors defines the relative velocity vector \mathbf{g} :

$$\mathbf{g} = V_{C_2} - V_{C_2H_2}. \quad (1)$$

in the laboratory system, the center-of-mass frame moves with the velocity V_{CM} calculated with the masses of the reactants m_{C_2} and $m_{C_2H_2}$ to eqn (2). With respect to the dicarbon beam, this vector holds a fixed center-of-mass angle, Θ_{CM} , (eqn (3)).

$$V_{CM} = \sqrt{\frac{(m_{C_2} V_{C_2H_2})^2 + (m_{C_2H_2} V_{C_2})^2}{(m_{C_2} + m_{C_2H_2})^2}} \quad (2)$$

$$\Theta_{CM} = \arctan\left(\frac{m_{C_2H_2} V_{C_2}}{m_{C_2} V_{C_2H_2}}\right). \quad (3)$$

This gives, at our specific example as depicted in Fig. 5, the center-of-mass angles of 22.5° and 39.6° for the reactions of acetylene with dicarbon and atomic carbon, respectively. The center-of-mass velocity vector starts at the crossing point of the reactant beams and terminates at the center-of-mass of the system which is actually located on the relative velocity vector \mathbf{g} . Since we have two reactions—those of acetylene with dicarbon and atomic carbon—simultaneously, we also have to define two center-of-masses, $CM_{C_2H_2/C_2}$ and $CM_{C_2H_2/C}$, which are both located on the relative velocity vector \mathbf{g} (Fig. 5). These center-of-masses play a central role to discriminate if the signal at lower mass-to-charge ratios actually originates from reaction (R1), (R2), (R3), alone or a combination of these channels. To distinguish between these possibilities, we must have a closer look at the energetics of each reaction. This is carried out here exemplarily for the reaction (R1) assuming solely the most stable cyclic C_3H isomer is formed. The total, maximum available energy, E_{avl} , of the reaction, which can be released in translational energy of the reaction products, is simply the sum of the collision energy, E_c (eqn (5)), minus the reaction energy of the reaction, $\Delta_R G$:

$$E_{avl} = E_c - \Delta_R G \quad (4)$$

$$E_c = \frac{1}{2} \left(\frac{m_{C_2H_2} \times m_C}{m_{C_2H_2} + m_C} \right) (V_{C_2H_2}^2 + V_C^2). \quad (5)$$

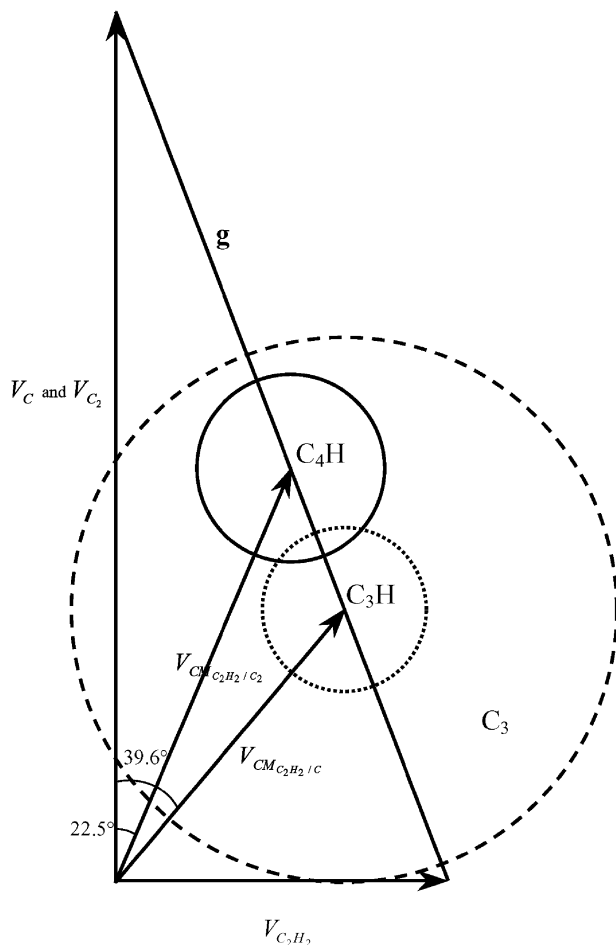


Fig. 5 Newton diagram of the reactions of carbon atoms and dicarbon molecules with acetylene *via* reactions $C(^3P_j) + C_2H_2 \rightarrow C_3H + H$ (R1), $C(^3P_j) + C_2H_2 \rightarrow C_3 + H_2$ (R2), and $C_2 + C_2H_2 \rightarrow C_4H + H$ (R3). The maximum recoil velocities of the butadiynyl (C_4H), tricarbonhydride (C_3H), and tricarbon (C_3) are depicted as solid, dotted, and dashed circles. See text for a detailed definition of the symbols.

Momentum conservation dictates how the available energy will be partitioned among the C_3H and H reaction products. Here, the maximum velocity of the heavy fragment in the center-of-mass reference frame, u_{C_3H} , can be calculated *via* eqn (6):

$$u_{C_3H} = \sqrt{\frac{2m_H E_{avl}}{m_{C_3H}(m_{C_3H} + m_H)}} \quad (6)$$

This presents the maximum recoil velocity a C_3H product can have in the center-of-mass system. Theoretically, the product molecules can scatter in a sphere which is centered at the center-of-mass of the reaction; this sphere holds a *radius* of a velocity vector μ_{C_3H} . Projecting the sphere into the two-dimensional velocity vector diagram (Fig. 5) around the center-of-mass of the reaction yields a circle with a *radius* of μ_{C_3H} (dotted circle). A similar procedure can be carried out to calculate the maximum recoil velocities of the tricarbon product and of the butadiynyl radical. A detailed inspection of these recoil circles, the so-called *Newton Circles*, provides vital guidance for the experiment. Let us follow a line from the crossing point of the ablation and the acetylene beam

along the center-of-mass of the velocity vector of the dicarbon plus acetylene reaction—placed 22.5° relative to the dicarbon vector—to the center-of-mass of the reaction. Here, we will see that this line passes first the Newton circle of the tricarbon reaction product and then the Newton circle of the butadiynyl radical. Most importantly, this line does not cross the Newton circle of the C₃H reaction product. Therefore, the time-of-flight spectra of butadiynyl recorded at $m/z = 49$ (C₄H⁺) and its fragmentation patterns can show only interference from the tricarbon reaction product ($m/z = 36$ and lower). Hence, the signal at $m/z = 37$ comes predominantly—except an isotopic contribution of 3.3% from ¹³C¹²C₂⁺—from fragmentation of the butadiynyl radical.

4. The computational approach

All *ab initio* calculations of the reactants, products, intermediates and transition states on the PESs of the C₂(¹Σ_g⁺/³Π_u) reactions with acetylene, ethylene, allene, and methylacetylene were carried out using the G2M(CC,MP2) method,³⁴ which approximates the CCSD(T)/6-311 + G(3df,2p) energy.³⁵ The geometries of various species were optimized at the density functional B3LYP/6-311G** level.^{36,37} Vibrational frequencies calculated at this level were used for characterization of stationary points as minima and transition states, for zero-point energy (ZPE) corrections, and for RRKM calculations of reaction rate constants. The GAUSSIAN 98³⁸ and MOLPRO 2002³⁹ *ab initio* program packages were employed. In this paper, we only focus on the computational results to supplement the experimental data. The complete triplet and singlet C₅H₄ surfaces are released in a forthcoming publication.⁴⁰ We would like to note that the electronic structure and statistical calculations (RRKM) cannot alone reveal the actual reaction mechanisms involved. The RRKM theory, for instance, presumes a complete energy randomization in the decomposing intermediate of a bimolecular reaction before the latter fragments. However, crossed beam studies of C(³P_j)/buta-1,2-diene,⁴¹ C(³P_j)/CD₃CCH,⁴² C(³P_j)/C₆H₆, C₆H₅/CH₃CCH,⁴³ and the reactions of electronically excited carbon atoms C(¹D₂) with acetylene, ethylene, and methylacetylene,^{44,45} revealed strong discrepancies between the predicted and the experimentally observed product distributions. In addition, potential energy surfaces cannot predict if the actual reaction is direct or indirect. On the other hand, electronic structure calculations provide guidance, if, for instance, experimental enthalpies of formation of radical products are missing. Therefore, crossed beam experiments and computations of the pertinent potential energy surfaces are highly complementary to expose the reaction dynamics of complicated, polyatomic reactions comprehensively.

5. Results

5.1. The dicarbon [C₂(X¹Σ_g⁺/a³Π_u)]-acetylene [C₂H₂(X¹Σ_g⁺)] system

To investigate the dynamics comprehensively, we performed the experiments at six collision energies ranging from 10.6 to 47.5 kJ mol⁻¹ (Table 1). Reactive scattering signal was monitored at mass-to-charge ratios of $m/z = 49$ (C₄H⁺), 48 (C₄⁺), 37 (C₃H⁺), and 36 (C₃⁺). TOF spectra at $m/z = 49$ (C₄H⁺) (Fig. 6), 48(C₄⁺), and 37 (C₃H⁺) overlapped after scaling at all laboratory angles and were fit with equal center-of-mass functions. Hence, the signal at $m/z = 48$ and 37 originates in cracking of the C₄H⁺ parent in the ionizer of the detector. Note, that TOFs recorded at $m/z = 36$ do not overlap with those at higher masses. Here, the signal at $m/z = 36$ originated from fragmentation of the C₄H⁺ parent to C₃⁺ in the ionizer and also from the C₃(X¹Σ_g⁺) + H₂(X¹Σ_g⁺) channel,³³ the latter pathway is accessible in bimolecular reactions of atomic carbon, C(³P_j) with acetylene.⁴⁶ Consequently, the time-of-flight data alone indicates the presence of a dicarbon *versus* atomic hydrogen exchange route which yields C₄H isomer(s) in the present experiments. At each collision energy, we can now integrate the TOF spectra to provide the laboratory angular distributions (LAB) of the C₄H product isomer(s) at $m/z = 49$ (C₄H⁺). The most probable Newton diagram and the corresponding laboratory angular distributions of the heavy C₄H product(s) recorded are displayed in Fig. 10 at a representative collision energy of 39.9 ± 0.2 kJ mol⁻¹. The LAB distribution is relatively narrow and spreads only to about 35° in the scattering plane. Also, the shape of the distributions change significantly as the collision energy rises. At lower collision energies of 10.6 ± 0.1 kJ mol⁻¹, 12.1 ± 0.2 kJ mol⁻¹, and 21.6 ± 0.2 kJ mol⁻¹, the LAB distribution

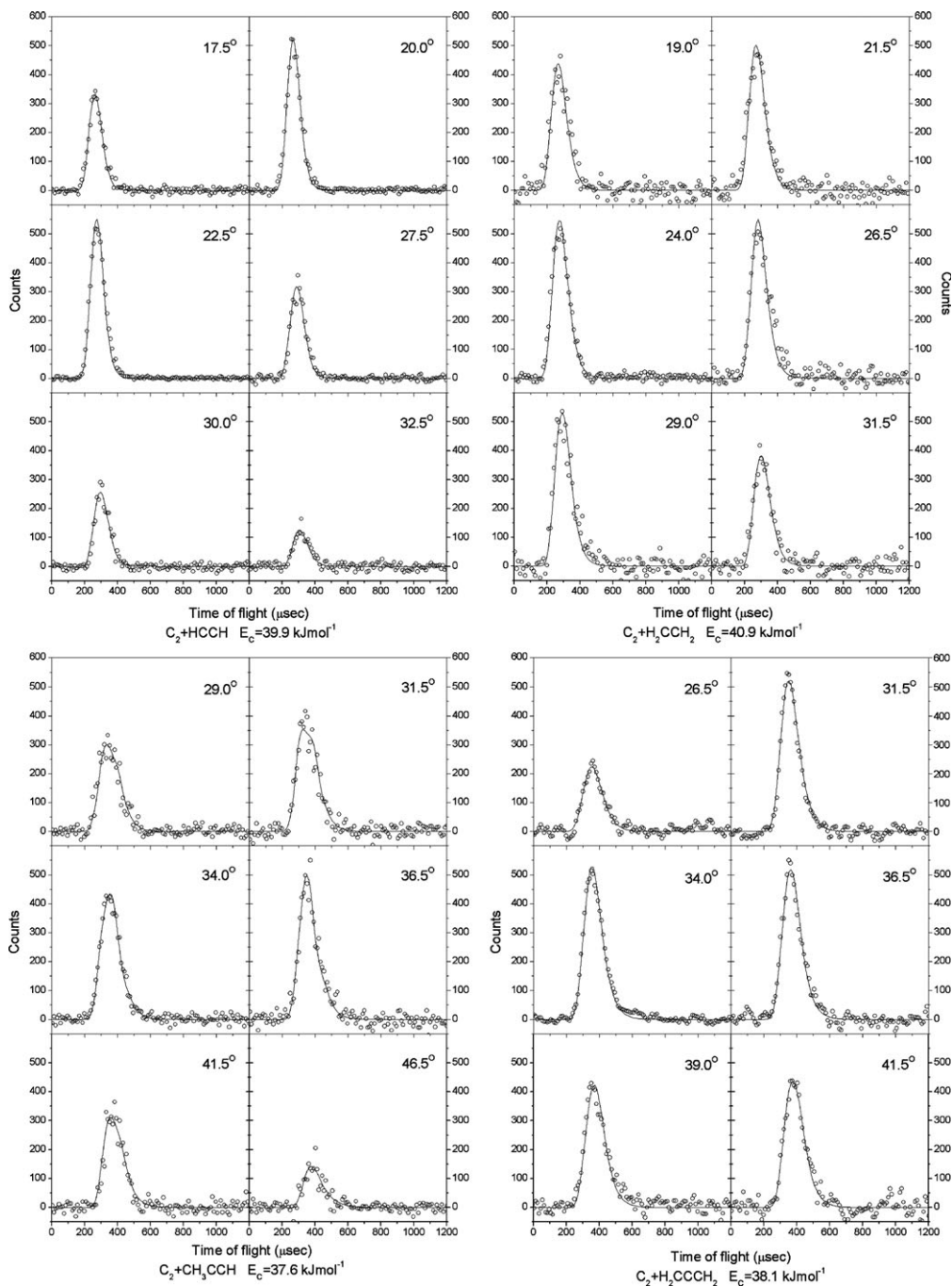


Fig. 6 Selected time-of-flight spectra (TOF) of the heavy hydrocarbon radical products of the generic formulae C_4H (acetylene reactant), C_4H_3 (ethylene reactant), and C_5H_3 (methylacetylene and allene reactants) recorded at the most intense mass-to-charge ratios (m/z) of $m/z = 49$ (C_4H^+), 50 ($C_4H_2^+$), and 62 ($C_5H_2^+$).

are forward scattered with respect to the dicarbon beam. As the collision energies increase, the LAB distributions become less forward scattered. A distinct switching from a forward- to a backward-scattered distribution is clearly visible at a collision energy of 29.0 ± 0.5 kJ mol^{-1} . The trend

actually amplifies by rising the collision energy even higher *via* $39.9 \pm 0.2 \text{ kJ mol}^{-1}$ to $47.5 \pm 1.2 \text{ kJ mol}^{-1}$. Most importantly, a best fit of the TOF spectra and of the LAB distribution could be achieved with only one pathway; the inherent center-of-mass translational energy distributions suggest an experimentally determined reaction exoergicity to form the C_4H isomer(s) plus atomic hydrogen of $39.9 \pm 5.0 \text{ kJ mol}^{-1}$ averaged over all six collision energies. Also, the flux contour map (Fig. 7) holds a maximum peaking away from zero velocity, *i.e.* $3\text{--}17 \text{ kJ mol}^{-1}$. These data suggest that at least one reaction channel exhibits an exit barrier and, hence, a significant geometry as well as electron density change from the fragmenting C_4H_2 intermediate to the products resulting in a repulsive bond rupture from a tight transition state. We also calculated the averaged fraction of the energy released into the translational degrees of the products to be $33 \pm 3\%$ —almost invariant on the collision energy (Fig. 8). Finally, the angular part of the flux contour maps clearly indicates intensity over the angular range from 0° to 180° (Fig. 7). This finding indicates indirect scattering dynamics through C_4H_2 complex(es).

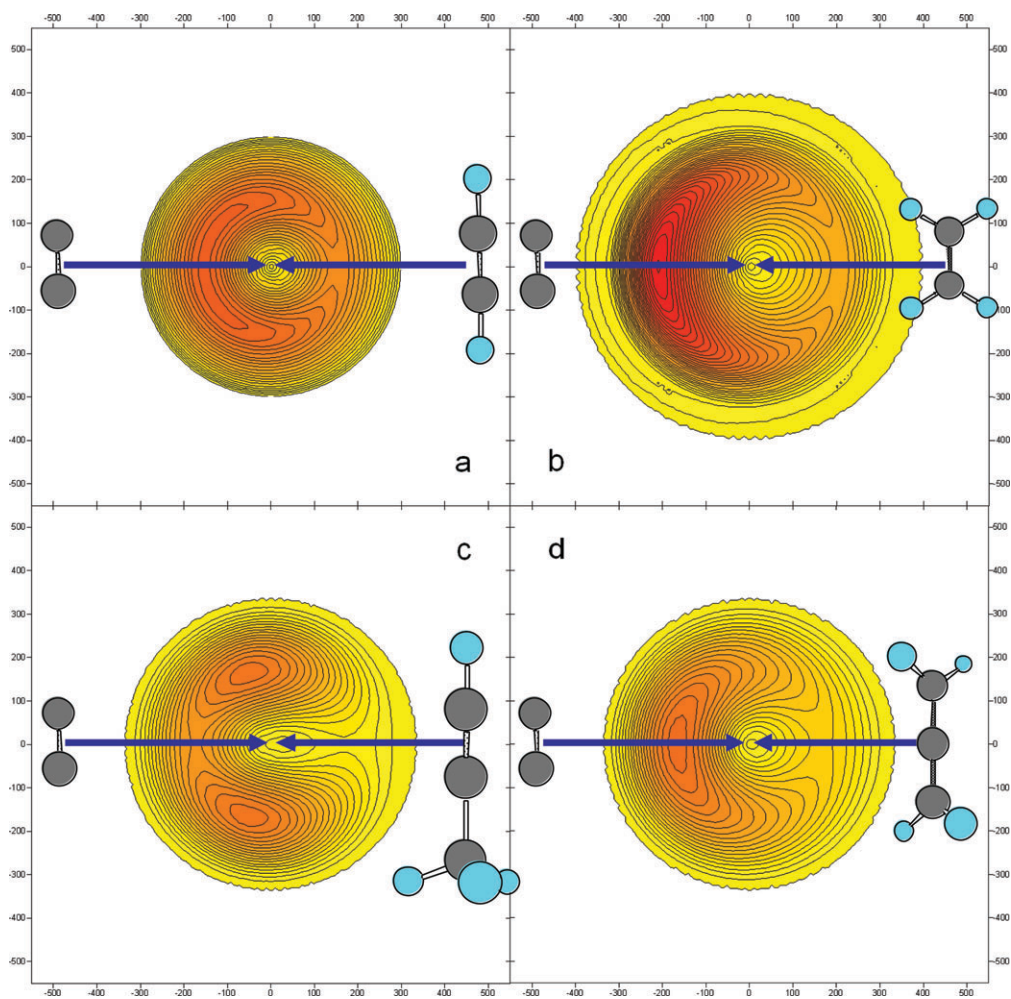


Fig. 7 Flux contour plots of the C_4H (acetylene reactant (a)), C_4H_3 (ethylene reactant (b)), and C_5H_3 (methylacetylene (c) and allene reactants (d)) radical product at selected collision energies. The solid lines connect data points with identical fluxes.

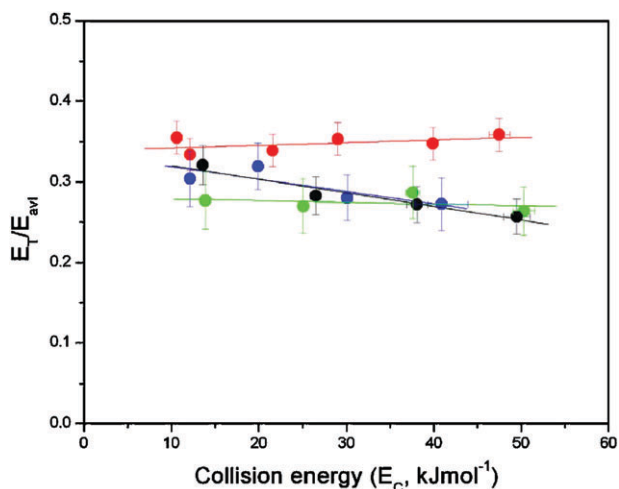


Fig. 8 Collision energy dependence of the fraction of the available energy channeled into the translational motion of the C_4H (acetylene reactant (red)), C_4H_3 (ethylene reactant (blue)), and C_5H_3 (methylacetylene (green) and allene reactants (black)) plus atomic hydrogen products.

5.2. The dicarbon [$C_2(X^1\Sigma_g^+ / a^3\Pi_u)$]-ethylene [$C_2H_4(X^1A_g)$] system

The reaction of dicarbon with ethylene was conducted at four distinct collision energies between 12.1 and 40.9 kJ mol^{-1} (Table 1). At each collision energy, the signal was recorded of the parent ion at $m/z = 51$ ($C_4H_3^+$) and of the fragments at $m/z = 50$ ($C_4H_2^+$), $m/z = 49$ (C_4H^+), $m/z = 48$ (C_4^+). TOF spectra at mass-to-charge ratios between $m/z = 51$ and 48 were superimposable; therefore, the signal at $m/z = 50$ –48 originates from cracking of the parent ion in the electron impact ionizer. This suggests the formation of C_4H_3 isomer(s) *via* a dicarbon *versus* atomic hydrogen replacement pathway. A typical laboratory angular distribution is reported in Fig. 10 recorded at the $m/z = 50$ fragment at a collision energy of 40.9 kJ mol^{-1} . As the collision energy rises, the shape of the laboratory angular distributions changes from a forward-backward symmetry to an increasingly backward peaking. The best fits of each LAB distribution together

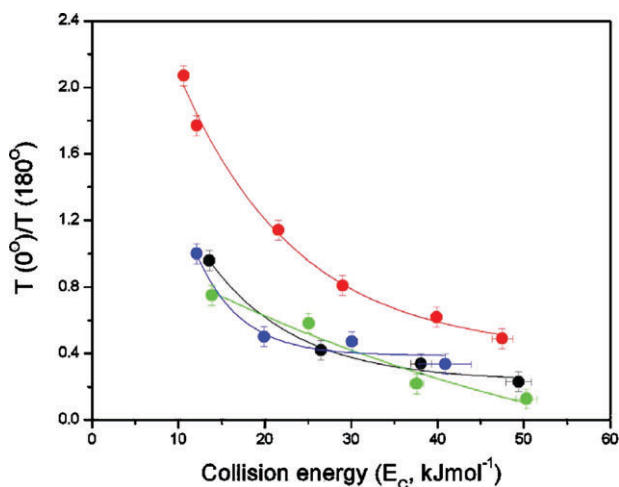


Fig. 9 Collision energy dependence of the ratio of the center-of-mass angular distributions at the poles, $T(0^\circ)/T(180^\circ)$, of the C_4H (acetylene reactant (red)), C_4H_3 (ethylene reactant (blue)), and C_5H_3 (methylacetylene (green) and allene reactants (black)) plus atomic hydrogen products.

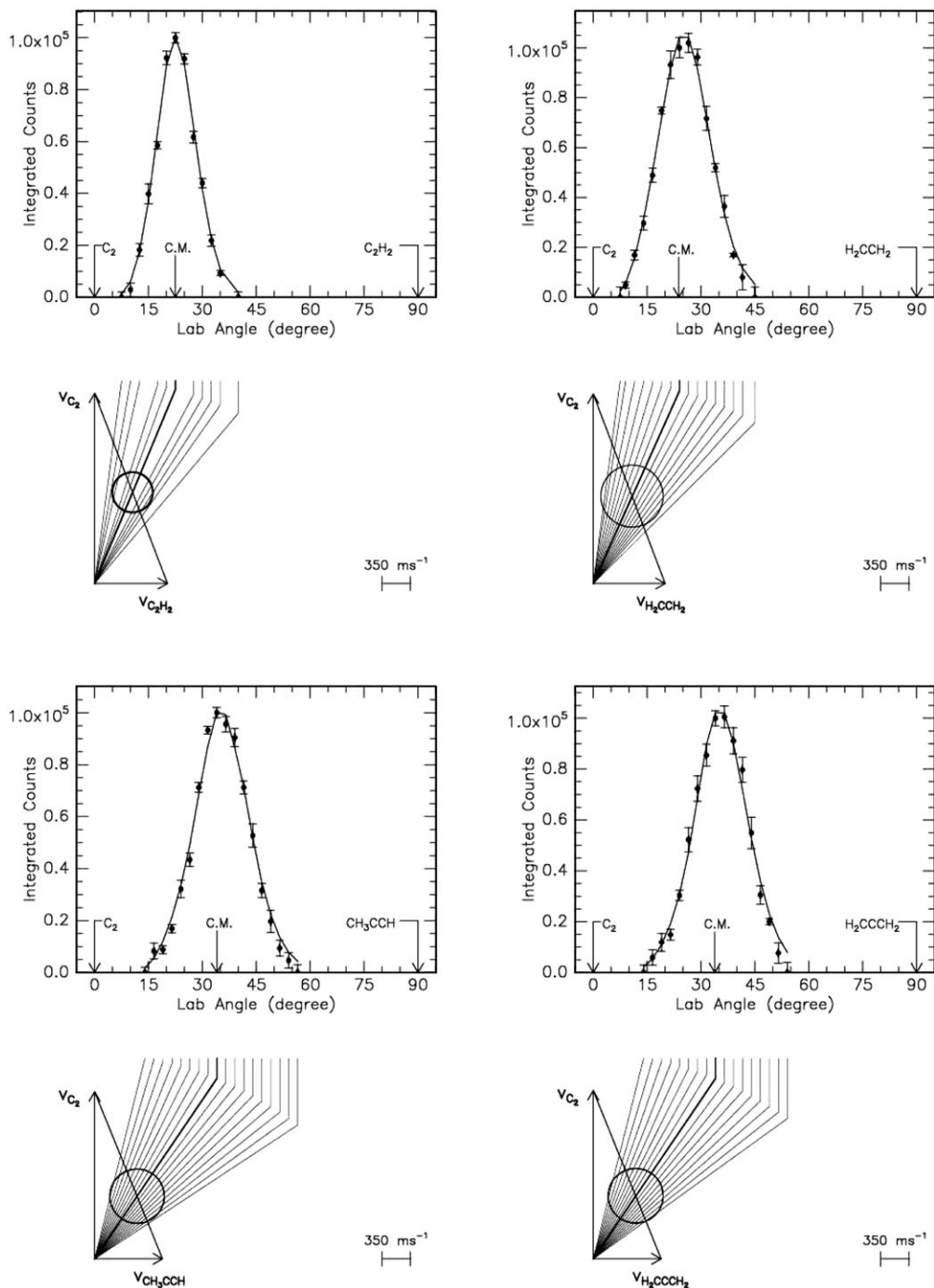


Fig. 10 Selected Newton diagrams and laboratory angular distributions for the reactions of dicarbon with acetylene, ethylene, methylacetylene, and allene. The LAB distributions of the heavy hydrocarbon radicals of the generic formulae C_4H (acetylene reactant), C_4H_3 (ethylene reactant), and C_5H_3 (methylacetylene and allene reactants) were obtained by integrating the corresponding TOF spectra recorded at the most intense mass-to-charge ratios (m/z) of the radicals at $m/z = 49$ (C_4H^+), 50 ($C_4H_2^+$), and 62 ($C_5H_2^+$).

with the TOF spectra (Fig. 6) could be conducted with one channel and a single translational energy distribution extending to 180–220 kJ mol⁻¹. Fig. 7 also shows the resulting flux contour map at a selected collision energy. Since the maximum energy released is the sum of the reaction exoergicity and the collision energy, we are able to determine the reaction exoergicity needed to form the C₄H₃ isomer(s) plus atomic hydrogen as 175 ± 10 kJ mol⁻¹ averaged over four collision energies. Also, as is obvious from the contour map (Fig. 7), the flux of the C₄H₃ isomer(s) shows a maximum away from zero; this broad plateau correlates with translational energies of between 5 and 45 kJ mol⁻¹. Hence, at least one pathway to synthesize the C₄H₃ isomer(s) likely holds a tight exit transition state. Finally, an inspection of the flux contour maps indicates intensity over the angular range from 0° to 180° suggesting that the reaction mechanism is indirect and proceeds *via* a bound C₄H₄ complex.

5.3. The dicarbon [C₂(X¹Σ_g⁺/a³Π_u)]-methylacetylene [CH₃CCH(X¹A₁)] system

The crossed beams experiments were carried out at four different collision energies between 13.9 and 50.3 kJ mol⁻¹ (Table 1). At each experiment, we observed reactive scattering signal at mass-to-charge ratios of $m/z = 63$ (C₅H₃⁺), 62 (C₅H₂⁺), 61 (C₅H⁺), and 60 (C₅⁺). Time-of-flight spectra (TOF) for several scattering angles at a selected collision of 37.6 kJ mol⁻¹ are shown in Fig. 6. Note, that the TOF spectra at mass-to-charge-ratios between 63 and 60 reveal identical patterns proposing that $m/z = 63$ fragments to yield signals at $m/z = 62$ –60. The overlapping patterns of the lower mass-to-charge ratios further suggest that in this range of masses only the dicarbon *versus* hydrogen exchange pathway is open to form C₅H₃ isomer(s) ($m/z = 63$) plus atomic hydrogen; based on these data the formation of any C₅H₂ isomers ($m/z = 62$) plus molecular hydrogen can be ruled out. For completeness, we also investigated the signal at lower mass-to-charge ratios. Here, no signal was found at $m/z = 52$ (C₄H₄⁺) indicating that the reaction to form any C₄H₄ isomers plus atomic carbon is closed. Time-of-flight spectra taken between $m/z = 51$ (C₄H₃⁺) and 48 (C₄⁺) have to be fit with two channels: a contribution from the reaction of dicarbon with methylacetylene (dissociative ionization of C₅H₃ in the electron impact ionizer) and from the participation of the scattering signal of atomic carbon plus methylacetylene reaction forming atomic hydrogen plus the but-1-en-3-yn-2-yl radical (i-C₄H₃(X²A')) giving rise to its parent at C₄H₃⁺ ($m/z = 51$) and the C₄H₂⁺ ($m/z = 50$), C₄H⁺ ($m/z = 49$), and C₄⁺ ($m/z = 48$) fragments. Based on the data, the TOF spectra imply the presence of a dicarbon *versus* atomic hydrogen exchange pathway and also the synthesis of C₅H₃ isomer(s) under single collision conditions. The TOF spectra can now be integrated to obtain one laboratory angular distribution (LAB) of the C₅H₃ product(s) at the most intense m/z value of 62 (C₅H₂⁺) for each collision energy. Fig. 10 depicts a selected LAB distribution at a collision energy of 37.6 kJ mol⁻¹. Summarized, the LAB distributions of the C₅H₃ isomer(s) at $m/z = 62$ peak close to the center of mass angles of the reactions. The overall shapes show a slight backward-scattered distribution prolonging between 40°–45° in the scattering plane as defined by both beams. Note, that as the collision energy increases, the LAB distributions become more backward scattered. The best fit of each LAB distribution and of the TOF spectra was carried out with only one channel and a translational energy distribution extending to 180–230 kJ mol⁻¹; the flux contour maps at this selected collision energy is shown in Fig. 7. Recalling that the maximum energy releases is simply the sum of the reaction exoergicity plus the collision energy; therefore, we can subtract the latter from the high energy cutoff to obtain an experimental reaction exoergicity to synthesize the C₅H₃ isomer(s) plus atomic hydrogen. Averaging over all four collision energies, an averaged value of 181 ± 12 kJ mol⁻¹ is derived. As can be seen from the flux contour map (Fig. 7), the flux of the C₅H₃ isomer(s) peaks away from zero velocity; the relatively broad peak correlates with center-of-mass translational energies between 15 and 40 kJ mol⁻¹. This proposes that at least one reaction channel to form the C₅H₃ isomer(s) has a tight exit transition state (repulsive carbon–hydrogen bond rupture involving a significant electron rearrangement). Finally, the translational energy part of the flux contour map allows us to determine the averaged fraction of the energy released into the translational degrees of the products to be about 27 ± 2%—almost independent on the collision energy (Fig. 8). This order-of-magnitude suggests that the reaction proceeds in an indirect fashion *via* complex formation.⁴⁷ Also, a detailed look of the angular parts of the flux contour maps depict intensity over the angular range from 0° to 180°; this involves

indirect scattering dynamics and the participation of at least one C_5H_4 complex in the entrance channel (Fig. 7).

5.4. The dicarbon [$C_2(X^1\Sigma_g^+ / a^3\Pi_u)$]-allene [$H_2CCCH_2(X^1A_1)$] system

We conducted the crossed beams reactions of allene with dicarbon at four different collision energies between 13.6 and 49.4 kJ mol^{-1} (Table 1). Similar to the dicarbon–methylacetylene system, the reactive scattering signal was detected at mass-to-charge ratios of $m/z = 63$ ($C_5H_3^+$), 62 ($C_5H_2^+$), 61 (C_5H^+), and 60 (C_5^+) at all collision energies. Fig. 6 portrays time-of-flight spectra (TOF) recorded at $m/z = 62$ at a collision energy of 38.1 kJ mol^{-1} as a typical example. At mass-to-charge ratios from 63 to 60, the TOF spectra showed overlapping profiles indicating that $m/z = 63$ fragments give signals at mass-to-charge ratios between $m/z = 62$ and $m/z = 60$. This finding indicates that solely the atomic hydrogen *versus* dicarbon replacement channel is open to give atomic hydrogen and C_5H_3 isomer(s) ($m/z = 63$). Also, signals at lower mass-to-charge ratios did not reveal any additional reaction pathways over the complete range of collision energies in the dicarbon plus allene system. Therefore, the time-of-flight data indicate the occurrence of a dicarbon *versus* atomic hydrogen replacement pathway together with the formation of C_5H_3 isomer(s) under single collision conditions as provided in crossed beams experiments. We can also integrate the TOF spectra to provide the laboratory angular distributions (LAB) of the C_5H_3 product(s) at the most intense m/z value of 62 ($C_5H_2^+$). A typical distribution is shown in Fig. 10 at a selected collision energy of 38.1 kJ mol^{-1} . All LAB distributions exhibited maxima in the vicinity of the center of mass angles of the bimolecular reactions. At the lowest collision energy of 13.6 kJ mol^{-1} , the distribution is isotropic (flat). With rising collision energy, however, these distributions show a pronounced backward-scattering (Fig. 7 and 9). At all collision energies, a best fit of the TOF spectra together with the LAB distribution was obtained with a single channel and translational energy distributions depicting high energy cutoffs at 190–230 kJ mol^{-1} . This yields an experimentally determined reaction exoergicity to form the C_5H_3 isomer(s) plus atomic hydrogen of 191 ± 11 kJ mol^{-1} averaged over all four collision energies. Note, that this flux contour map (Fig. 7) also has a maximum away from zero velocity peaking at corresponding translational energies between 10 and 45 kJ mol^{-1} . Again—similar to the dicarbon plus methylacetylene system—at least one reaction pathway to yield the C_5H_3 isomer(s) holds a tight exit transition. We can also inspect the averaged fraction of the energy released into the translational degrees of the products; this fraction drops slightly from $32 \pm 1\%$ to $25 \pm 1\%$ as the collision energy increases (Fig. 8). The order-of-magnitude indicates such that the reaction is indirect and involves at least one intermediate. This is supported by the angular parts of the flux contour maps having intensity over the angular range from 0° to 180° (Fig. 7).

6. Discussion

6.1. General trends

As evident from the time-of-flight spectra and from the LAB distributions together with the best-fit center-of-mass functions, the reactions of dicarbon with unsaturated hydrocarbons are dictated by a dicarbon *versus* atomic hydrogen exchange pathway to form unsaturated hydrocarbon radicals of the generic formulae C_4H (acetylene reactant), C_4H_3 (ethylene reactant), and C_5H_3 (methylacetylene and allene reactants). Note, that we could not observe any evidence of any molecular hydrogen elimination channel although any molecular loss route is detectable with our crossed beams machine as demonstrated explicitly in the atomic carbon–acetylene system.³³ To identify the nature of the reaction products and to assign the isomer product correctly, we examined the experimentally derived reaction energies and compared those data with the computed energies for distinct isomers. How can this goal be achieved? Remember if the energetics of the product isomers are well separated, the maximum translation energy E_{max} can be used to identify the nature of the products. Since E_{max} presents the sum of the reaction exoergicity plus the experimental collision energy, we subtracted the collision energy from E_{max} to ascertain the experimentally determined exoergicity of the reaction to be 40 ± 5 kJ mol^{-1} (C_4H), 175 ± 10 kJ mol^{-1} (C_4H_3), as well as 181 ± 12 kJ mol^{-1} (C_5H_3 ; methylacetylene reactant) and 191 ± 11 kJ mol^{-1} (C_5H_3 , allene reactant). These data agree nicely—within the error limits of the computations of ± 5 kJ mol^{-1} —with the calculated reaction

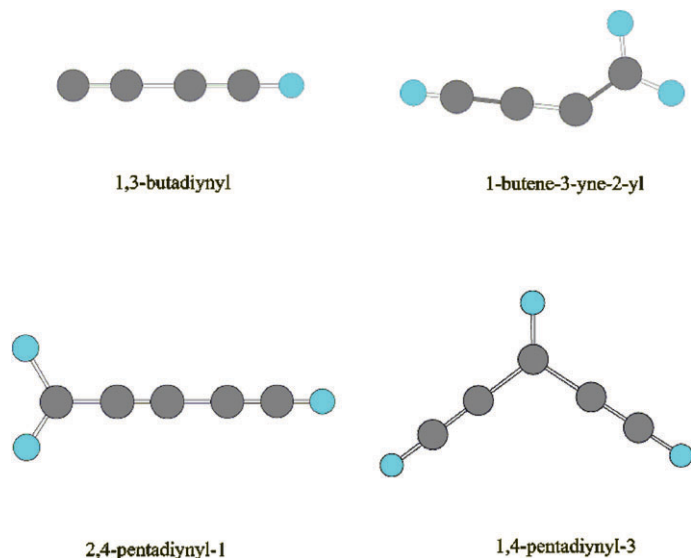


Fig. 11 Structures of the reaction products of dicarbon molecules acetylene, ethylene, allene, and methylacetylene: buta-1,3-diyanyl [$C_4H(X^2\Sigma^+)$ HCCCC], 1-butene-3-yne-2-yl [$i-C_4H_3(X^2A')$ H₂CCCCH], penta-2,4-diyanyl-1 [$C_5H_3(X^2B_1)$ HCCCCCH₂], and penta-1,4-diyanyl-3 [$C_5H_3(X^2B_1)$ HCCCCHCCH].

energies to form the buta-1,3-diyanyl [$C_4H(X^2\Sigma^+)$, HCCCC, acetylene reaction, $\Delta_r G = -33$ kJ mol⁻¹] and 1-butene-3-yne-2-yl [$i-C_4H_3(X^2A')$, H₂CCCCH, ethylene reaction, $\Delta_r G = -156$ kJ mol⁻¹]. The stated energetics are those computed for the singlet surface; those obtained on the triplet surface are slightly more exoergic and were calculated to be $\Delta_r G = -42$ kJ mol⁻¹ (acetylene reaction) and $\Delta_r G = -165$ kJ mol⁻¹ (ethylene reaction). Based on the energetics alone, the situation of the dicarbon–methylacetylene and dicarbon–allene systems is less clear. Here, both the experimentally obtained reaction energies can account for the formation of the penta-2,4-diyanyl-1 [$C_5H_3(X^2B_1)$, HCCCCCH₂] and penta-1,3-diyanyl-3 [$C_5H_3(X^2B_1)$ HCCCCHCCH] radical under single collision conditions since the enthalpies of formation of these radicals differ by only about 1 kJ mol⁻¹ (Fig. 11–15).

In addition, to the reaction energies, the distribution maxima of the $P(E_T)$ s provide—in the most favourable case—the order-of-magnitude of the barrier height in the exit channel. If, for instance, a $P(E_T)$ peaks at zero or close to zero, the bond rupture has either no or only a small exit barrier (loose exit transition state). On the other hand, the $P(E_T)$ s could show pronounced maxima away from zero translational energy; this may suggest a considerable electron density change from the fragmenting intermediate to the products and hence a tight transition state from the decomposing intermediate to the products. Considering the best fits, all center-of-mass translational energy distributions depict pronounced peaks in the range of 3–17 kJ mol⁻¹ (dicarbon–acetylene), 5–45 kJ mol⁻¹ (dicarbon–ethylene), 15–40 kJ mol⁻¹ (dicarbon–methylacetylene), and 10–45 kJ mol⁻¹ (dicarbon–allene). In case of the ethylene reaction, in particular, the distribution maxima are very broad and spread over 40 kJ mol⁻¹; this likely suggests the existence of two microchannels from the singlet and triplet surface. Note, that on each singlet potential energy surface, the exit transition states for the atomic hydrogen emission are mostly loose; on the other hand, on the triplet surface, the intermediates involve primarily tight exit transition states (Fig. 12–15).

We can also analyze the energy dependence of the averaged fraction of the available energy released into the translational degrees of the reaction products in detail (Fig. 8). In all reactions investigated, this fraction is limited within a relatively narrow range from 28% to only 35% and only slightly dependent on the collision energy. This order of magnitude suggests that the reactions are indirect and involve initially the formation of collision complexes.^{8,26} Recall that for direct reactions, typical fractions of 50% to 60% are reasonable limits.

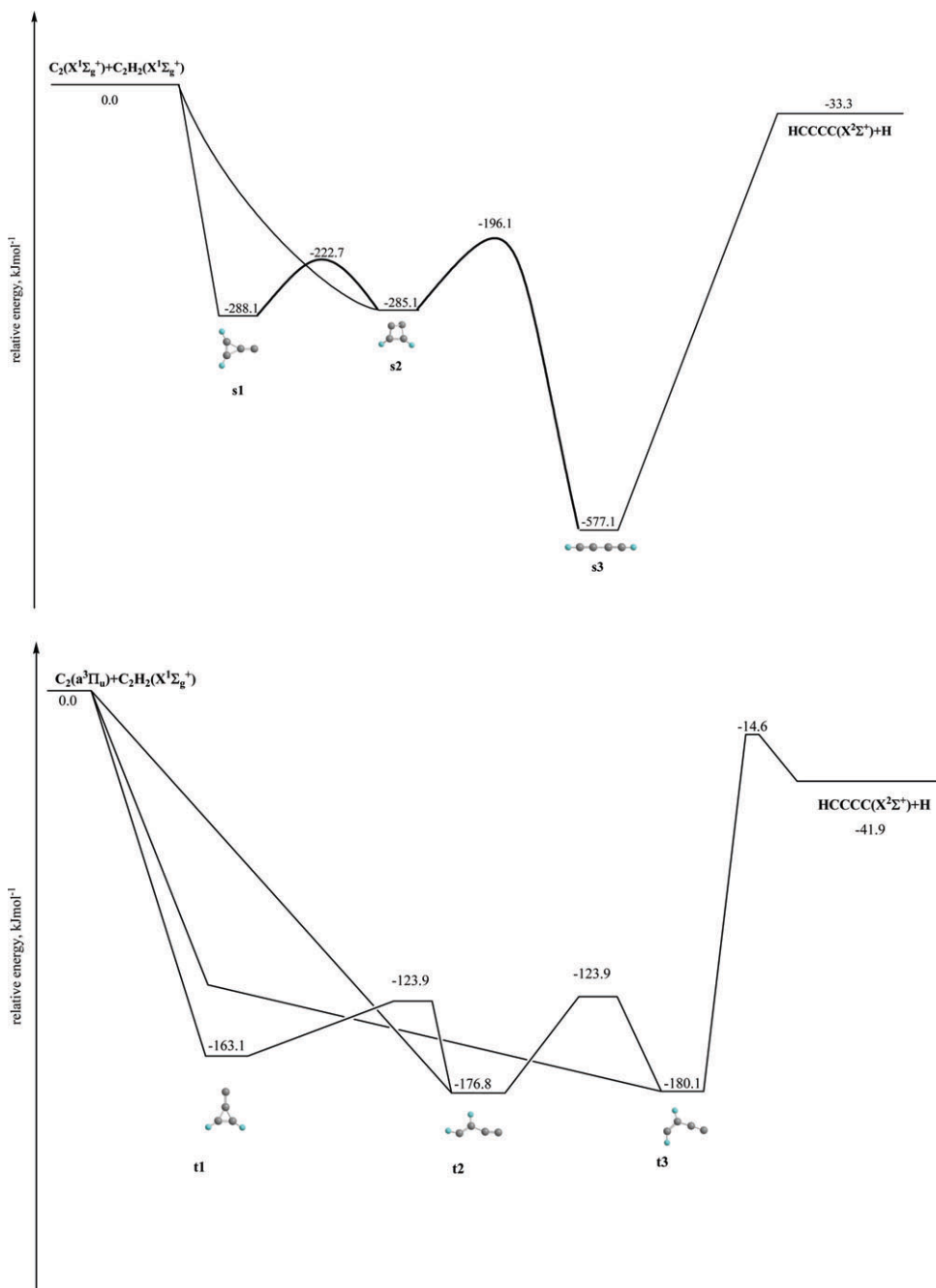


Fig. 12 Simplified potential energy surface (PES) of the reactions of ground state and electronically excited dicarbon molecules with acetylene.

The center-of-mass angular distributions provide additional knowledge on the underlying reaction dynamics and on the intermediates involved. The detailed shape of the $T(\theta)$ is dictated by the disposal of the total angular momentum. In principle, various shapes of the flux distributions are feasible. First, the $T(\theta)$ s can portray a symmetric profile around 90° . This ‘forward–backward’

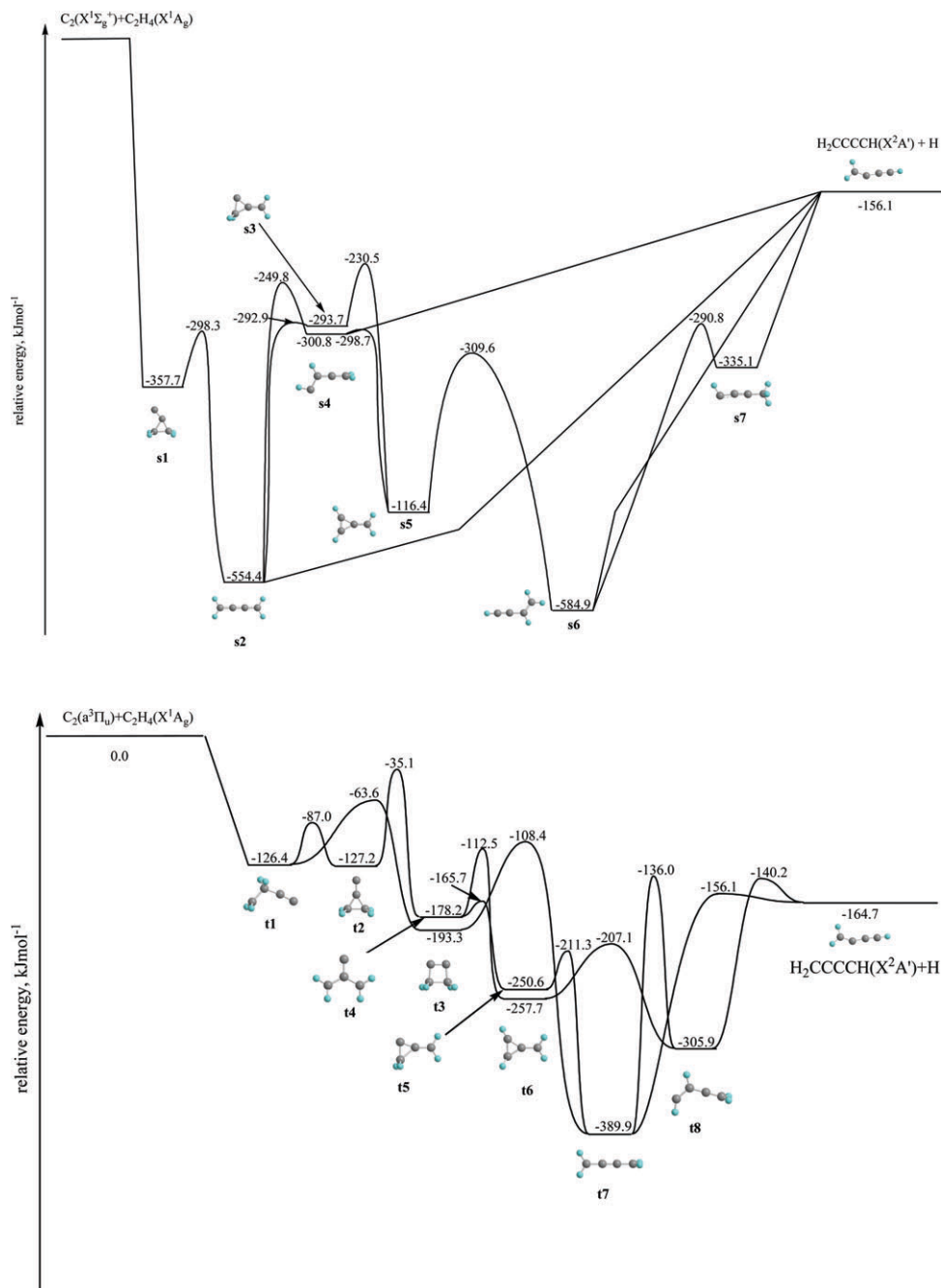


Fig. 13 Simplified potential energy surface (PES) of the reactions of ground state and electronically excited dicarbon molecules with ethylene.

symmetric pattern is characteristic for a bimolecular reaction which goes through an intermediate (indirect scattering dynamics) having a lifetime larger than its rotation period. Alternatively, a symmetric distribution around 90° could be interpreted in a way that the reaction involves a 'symmetric' reaction intermediate. In this case, the decomposing complex must have a rotation axis

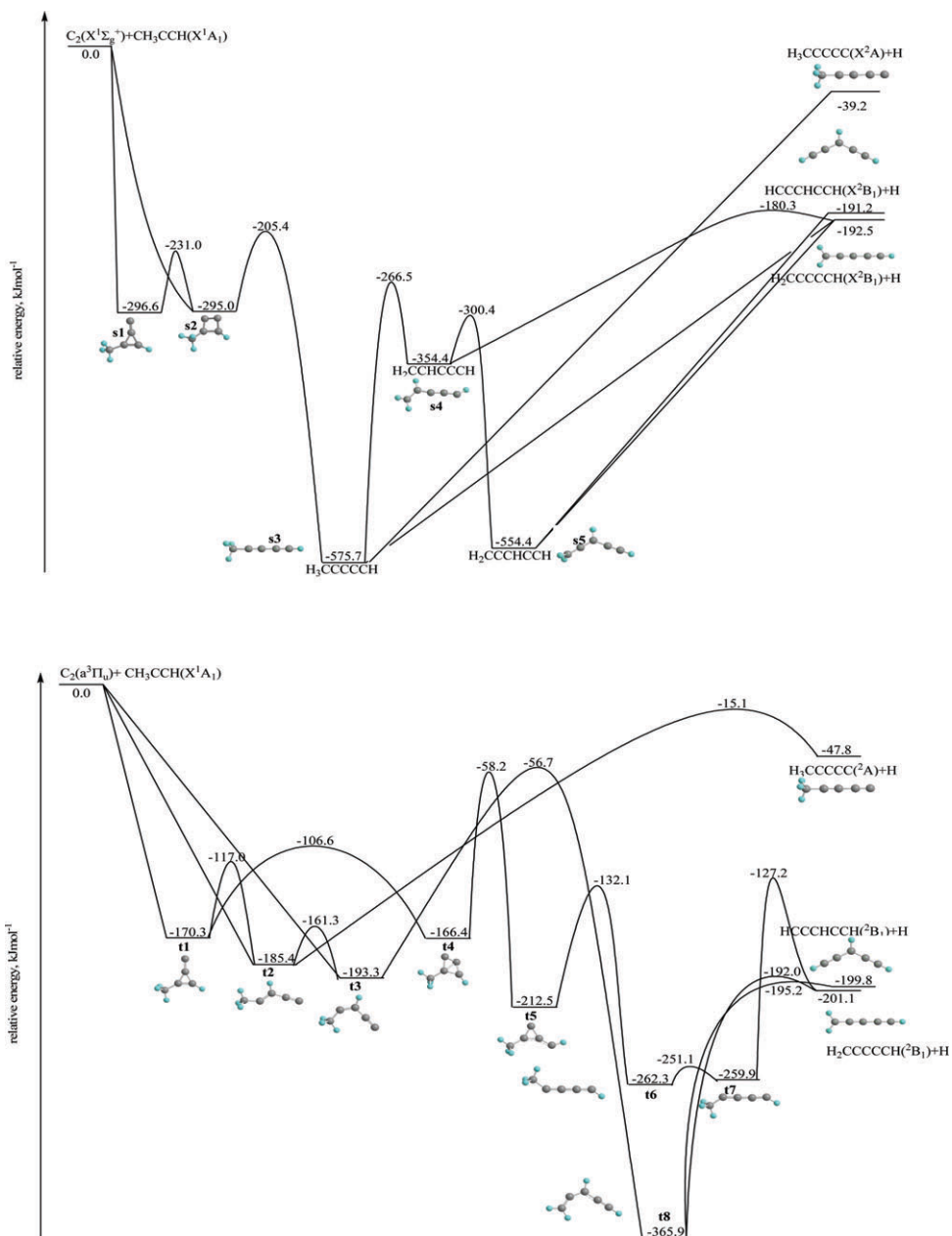


Fig. 14 Simplified potential energy surface (PES) of the reactions of ground state and electronically excited dicarbon molecules with methylacetylene.

which can interconvert, for instance, two hydrogen atoms *via* a proper rotation around a C_2 rotation axis. In this case, the chance of a hydrogen atom leaving the fragmenting intermediate into θ and $\pi - \theta$ is equal; this results in a forward–backward symmetric profile and even the intermediate has a lifetime shorter than its rotational period.⁸ Otherwise, the angular flux distribution can be asymmetric around 90° . Often, the flux at 0° or 180° is larger than at 180° or 0° , respectively, suggesting a so-called ‘osculating complex model’: the reaction is indirect, but the lifetime of the intermediate is in the order of the rotation period. Indirect reactions are frequently related with the

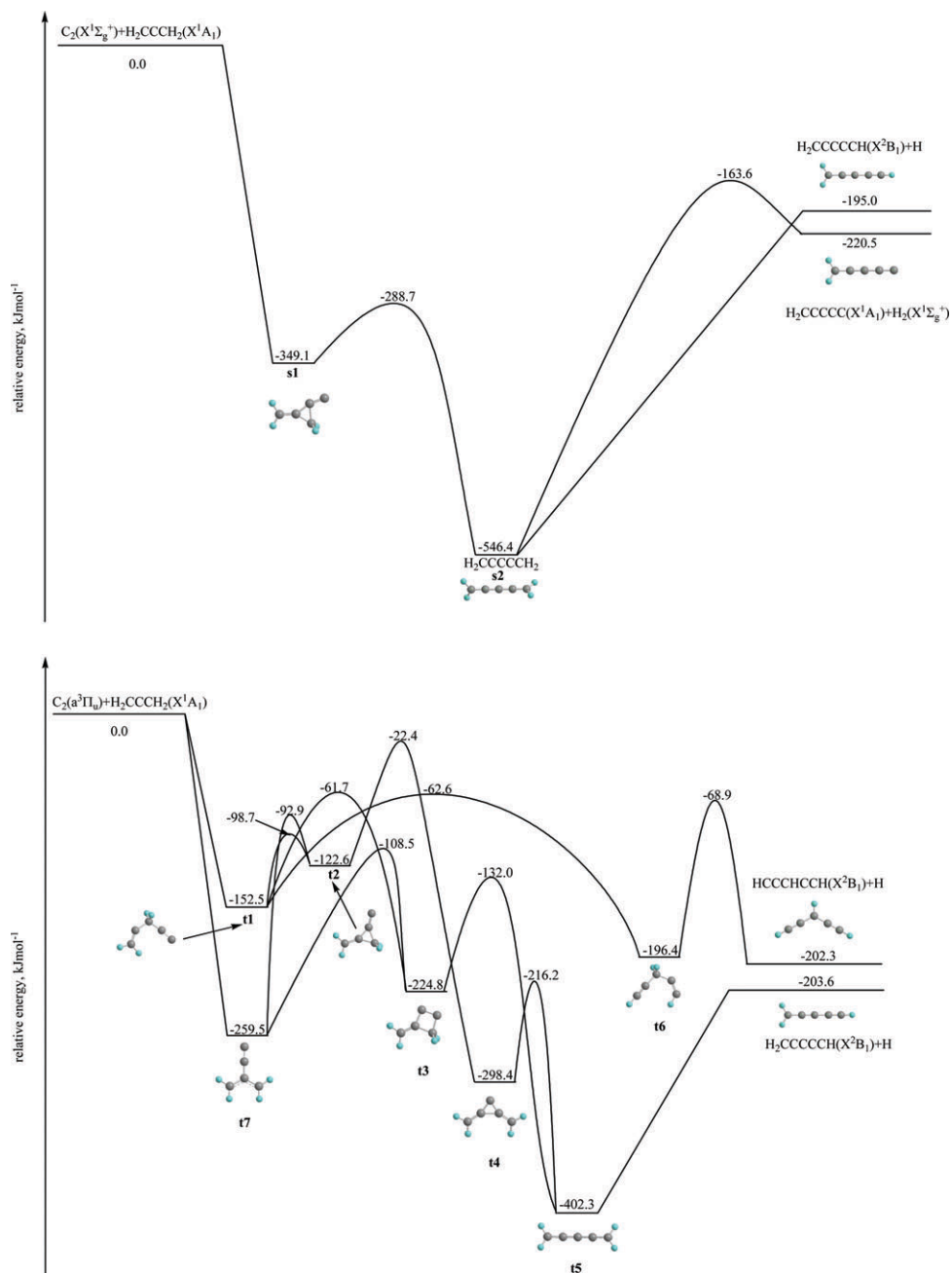
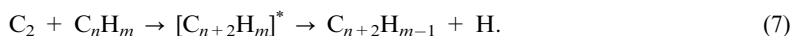


Fig. 15 Simplified potential energy surface (PES) of the reactions of ground state and electronically excited dicarbon molecules with allene.

deep potential energy well of a bound intermediate. Finally, the center-of-mass angular distribution might depict flux only in the forward direction, *i.e.* the flux peaks at 0° and is zero at larger angles ('stripping dynamics'), or only in the backward direction, *i.e.* the flux distribution shows a maximum at 180° and falls down to zero at lower angles ('rebound dynamics'). In these cases, the reaction is 'direct' and proceeds either *via* a very short lived, highly rovibrationally excited

intermediate with a lifetime of less than 0.1 ps, or goes through a transition state without involving an intermediate. Direct reactions are often associated with repulsive or weakly attractive potential energy surfaces. Here, we focus on the results which are relevant to help to understand the chemical evolution of circumstellar envelopes and of cold molecular clouds.

Most importantly, the center-of-mass angular distributions and the corresponding flux contour plots depict intensity over the complete angular range for each system (Fig. 7 and 9). This finding clearly demonstrates that the dynamics of the dicarbon plus unsaturated hydrocarbon reactions are indirect and proceed *via* complex formation (primary reaction intermediate). This complex, formally denoted as $[C_{n+2}H_m]^*$ in eqn (7) is—due to energy and total angular momentum conservation—rovibrationally excited, decomposes back to the initial reactants, fragments to the $C_{n+2}H_{m-1}$ product *via* atomic hydrogen elimination, or isomerizes (possibly *via* multiple steps) prior to its fragmentation. Together with the experimentally observed atomic hydrogen displacement channel, the chemical reaction can be therefore summarized in reaction (7). Also, the energy dependence of the $T(\theta)$ s, in particularly the increasingly backward-scattered shapes (Fig. 9) in combination with the electronic structure calculations (Fig. 12–15), can help us to collect additional information on the underlying reaction dynamics on the formation of the hydrocarbon radicals. Here, this energy dependence indicates the likely existence of two reaction channels, one pathway on the singlet surface and a second reaction on the triplet surface. This seems a plausible conclusion because the dicarbon beam contains dicarbon in its electronic ground state $C_2(X^1\Sigma_g^+)$ and also in the first electronically excited state $C_2(a^3\Pi_u)$.



6.2. The dicarbon $[C_2(X^1\Sigma_g^+/a^3\Pi_u)]$ -acetylene $[C_2H_2(X^1\Sigma_g^+)]$ system

In case of the dicarbon–acetylene reaction, the verification of the buta-1,3-diyanyl $[C_4H(X^2\Sigma^+), HCCCC]$ radical product requires the existence of a decomposing singlet diacetylene intermediate (**s3**) (Fig. 12–15). However, the latter belongs to the $D_{\infty h}$ point group and holds an infinite number of C_2 rotation axis perpendicularly to the molecular axis. Based on the arguments above, the $T(\theta)$ from the singlet surface should be always forward–backward symmetric since both hydrogen atoms can be interconverted *via* a rotation around 180° . Consequently, singlet diacetylene cannot account for the forward peaking at lower, but backward-peaking of the center-of-mass angular distributions at higher collision energies (Fig. 9). However, the triplet surface can account for these dynamics. Electronic structure calculations suggest the existence of three possible reaction intermediates **t1**–**t3**. Among them, intrinsic reaction coordinate calculations depict that only **t3** can decompose to the experimentally observed buta-1,3-diyanyl radical. Since the reaction has no entrance barrier, the maximum impact parameter leading to reaction actually decreases as the collision energy increases. Therefore, at lower collision energies, larger impact parameters could dominate the dynamics; this would involve the initial formation of **t2** followed by isomerization to **t3** (or the formation of **t3** in one step from the reactants) and decomposition to the fragments. In intermediate **t3**, both the attacking dicarbon unit and the leaving hydrogen atom are on opposite sides of the rotational axis of the intermediate. Also, **t2** and **t3** reside in relatively shallow potential energy wells; this might be responsible for a lifetime of the decomposing complex shorter than its rotational period and hence a deviation from a forward–backward symmetric profile. These findings can together explain the forward-peaking of the center-of-mass angular distributions at lower collision energies. However, as the collision energy rises, small impact parameters become more significant. This could lead to an enhanced formation of the cyclic intermediate **t1**; the latter isomerizes *via* **t2** and **t3** prior to its decomposition. This might correlate with a backward-scattered distribution of the buta-1,3-diyanyl radical. Summarized, on both the singlet and triplet surface, the dicarbon molecule adds to carbon–carbon triple bond of the acetylene molecule forming **s1/s2** (singlet surface) and **t1/t2/t3** (triplet surface; the ratio of **t1** versus **t2/t3** depends on the reactive impact parameters). These intermediates can isomerize eventually to **s3** and **t3**. The structures decompose through atomic hydrogen losses *via* loose (singlet) and tight (triplet) exit transition states. The existence of an exit barrier was already indicated by inspecting the center-of-mass translational energy distributions. Here, the peaking of the $P(E_T)$ s as much as 17 kJ mol^{-1} correlate nicely with an exit barrier on the triplet surface, here of

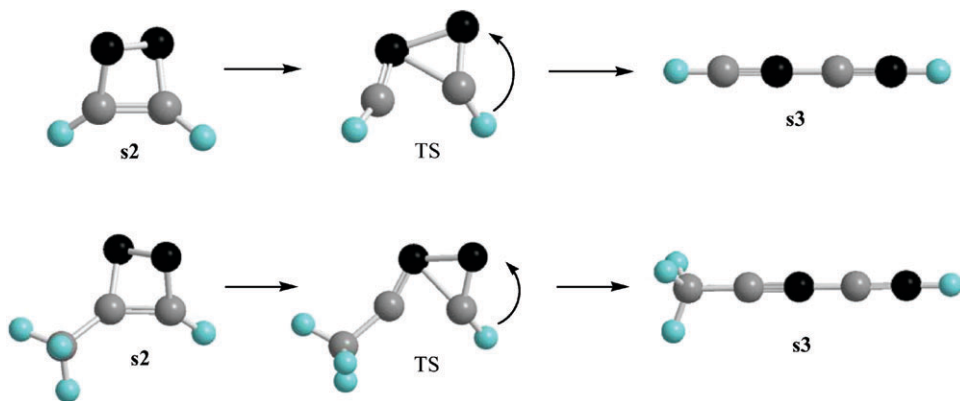


Fig. 16 Initial and final position of the carbon atoms in the reaction of the dicarbon molecule with acetylene (top) and methylacetylene (bottom) (black: carbon atoms of the dicarbon molecule; grey: carbon atoms of the hydrocarbon reactant) *via* opening of the tetracyclic ring intermediates **s2** *via* the transition states (TS) to the acyclic diacetylene and methyl diacetylene reaction products (**s3**) on the singlet surface.

about 26 kJ mol^{-1} . It is important to stress that both surfaces lead to the formation of the buta-1,3-diynyl radical [$\text{C}_4\text{H}(\text{X}^2\Sigma^+)$, HCCCC]. However, on the singlet and triplet surface, both radicals can be borne with distinctly different rovibrational excitation. On the singlet surface, our computations show that the isomerization from **s2** to **s3** involves a unique transition state (Fig. 16). Rather than being a formal insertion of the dicarbon unit into the carbon–carbon triple bond of the former acetylene molecule, the dicarbon molecule actually breaks up to yield a HCCCC intermediate **s3** (the carbon atoms of the dicarbon molecules are denoted in bold and italics) and hence HCCCC($\text{X}^2\Sigma^+$) and HCCCC($\text{X}^2\Sigma^+$) reaction products (Fig. 16). On the other hand, the triplet surface and **t1**–**t3** maintain the original dicarbon unit leading solely to HCCCC ($\text{X}^2\Sigma^+$) radicals. An experimental verification of these pathways is currently under way utilizing per- ^{13}C substituted acetylene.

6.3. The dicarbon [$\text{C}_2(\text{X}^1\Sigma_g^+/\text{a}^3\Pi_u)$]-ethylene [$\text{C}_2\text{H}_4(\text{X}^1\text{A}_g)$] system

The dicarbon–ethylene system shows more complicated reaction dynamics on the singlet and triplet surfaces. The formation of the C_s symmetric 1-butene-3-yne-2-yl radical [$\text{i-C}_4\text{H}_3(\text{X}^2\text{A}')$, H_2CCCCH] requires the existence of singlet and triplet butatriene intermediates **s2** and **t7**, respectively. Neither the initial collision complexes nor any reaction intermediate formed *via* successive isomerization of **s1** or **t1** can lose a hydrogen atom to synthesize the 1-butene-3-yne-2-yl isomer (Fig. 13). How can these complexes account for the symmetric center-of-mass angular distribution at lower, but increasingly backward scattered distributions as the collision energy increase? Recall that at the lowest collision energy, the forward–backward symmetry either suggests that the lifetime of **s2** and **t7** is longer than their rotational periods. Alternatively, a rotation of **s2** and **t7** around a C_2 axis can interconvert the leaving hydrogen atom; this would be reflected in a symmetric angular distribution although the lifetime of the decomposing intermediate(s) is actually shorter than its (their) rotation period. Since all principal axes of **s2** and **t7** coincide with C_2 rotational axes, we cannot discriminate if the symmetric center-of-mass angular distribution at lower energy is the result of the lifetime or of the symmetry of the molecules; experiments with d1 -substituted ethylene are underway to distinguish between both possibilities; here, the incorporation of a single deuterium atom decreases the symmetry of **s2** and **t7** from D_{2h} and D_{2d} to C_s in both cases; this eliminates the C_2 rotational axes and enables us to see if the forward–backward symmetry is maintained or not.

At higher collision energies, we still have to explain how the increasingly backward-scattered center-of-mass angular distributions can be accounted for. Recall that due to their symmetry, **s2** and **t7** all hold C_2 axes parallel to the A, B, and C principal rotational axes, and a fragmentation of these intermediates always results in forward–backward symmetric center-of-mass angular distributions.

Consequently, at least one additional decomposing intermediate must exist—either on the singlet or triplet surface—which does not have a C_2 rotational axis to interconvert two hydrogen atoms. On the singlet surface, **s4**, **s6**, and **s7** fulfil these requirements; these molecules can fragment without the exit barrier to form the 1-butene-3-yne-2-yl radical [*i*-C₄H₃(X²A'), H₂CCCCH]. On the other hand, **t8** also satisfies these conditions and may decompose *via* an exit barrier located 25 kJ mol⁻¹ above the separated products. Therefore, our electronic structure calculations and the existence of non-symmetric reaction intermediate(s) can account for the asymmetry in the center-of-mass angular distributions at higher collision energies. The explicit identification of the decomposing asymmetric molecule(s) is still in progress. All potential intermediates reside in relatively shallow potential energy wells; this could explain the asymmetric center-of-mass angular distribution and hence the inherent life time of the intermediates shorter than the(ir) rotational period. Also, recall that the center-of-mass translational energy distributions suggest the presence of an exit barrier; broad distribution maxima were found between 5–45 kJ mol⁻¹. On the other hand, the singlet and triplet potential energy surfaces suggest rather loose exit transition state with no (singlet) and only a moderate barrier of about 9 kJ mol⁻¹, (from **t7**), and the translation energy distributions should peak closer to zero.⁸ However, the involvement of **t8** could account for the off-zero peaking of the translational angular distributions.

6.4. The dicarbon [C₂(X¹Σ_g⁺/a³Π_u)-methylacetylene [CH₃CCH(X¹A₁)] system

Based on the energetics alone, we cannot decide if the penta-2,4-diynyl-1 [C₅H₃(X²B₁), HCCCCCH₂] and/or penta-1,4-diynyl-3 [C₅H₃(X²B₁) HCCCCHCCH] radical are formed under single collision conditions in the reaction of dicarbon with methylacetylene (Fig. 14). Recall that the enthalpies of formation of these isomers differ only by 1 kJ mol⁻¹; this difference is lower than the error limits of the experimentally determined reaction energy of ±12 kJ mol⁻¹. The potential involvement of a third isomer, H₃CCCCC(X²A), complicates the interpretation of the data even further. Here, the reaction to form this structure plus atomic hydrogen were determined to be -39 and -48 kJ mol⁻¹, respectively. To facilitate the identification of the product isomer, we also carried out an experiment utilizing CD₃CCH to investigate explicitly if the hydrogen atom is released from the methyl group or from the acetylenic carbon atom. Here, the decomposition of a CD₃C₄H intermediate (*m/z* = 67) could form CD₂C₄H (D atom loss; *m/z* = 65) or C₅D₃ (*m/z* = 66; H atom loss). Experimentally, we only observed a signal at *m/z* = 65, but not at *m/z* = 66. This verifies explicitly that the released atom is a deuterium atom. We can compare these experimental observations now with the computed singlet and triplet surfaces (Fig. 14). On the singlet surface, the formation of the H₃CCCCC(X²A) isomer requires the existence of a methylacetylene intermediate **s3**. Considering partially deuterated methylacetylene (d3-methylacetylene), this translates into a CD₃-C≡C-C≡C-H structure which had to lose a hydrogen atom forming D₃CCCCC(X²A). Since only a deuterium loss was observed experimentally, we can exclude the formation of D₃CCCCC(X²A) on the singlet surface. On the triplet surface, the synthesis of the H₃CCCCC(X²A) isomer had to involve the presence of intermediate **t2**. Again, in case of a d3-methylacetylene reactant (CD₃CCH), this process would lead to the emission of a hydrogen atom from the acetylenic group giving a signal solely at D₃CCCCC(X²A). Similar to the singlet surface, no hydrogen emission was observed, and the formation of D₃CCCCC(X²A) and hence—in case of methylacetylene—H₃CCCCC(X²A) can be ruled out. The exclusion of the hydrogen loss pathway has additional consequences for the triplet surface. Here, intermediate **t8** which can be formed *via* hydrogen shift from **t3** should fragment due to similar energetics and exit barrier heights to the penta-2,4-diynyl-1 [C₅H₃(X²B₁), HCCCCCH₂] and penta-1,4-diynyl-3 [C₅H₃(X²B₁) HCCCCHCCH] radical. In case of the d3-methylacetylene (CD₃CCH) reactant this translates into the formation of a D₂CCCHCCD **t8** intermediate formed *via* a deuterium shift from the d3-substituted **t3** isomer. A decomposition of D₂CCCHCCD **t8** should yield the d3-penta-2,4-diynyl-1 [C₅D₃, DCCCCCD₂] and d2-penta-1,4-diynyl-3 [C₅HD₂, HCCCDCCD] *via* atomic hydrogen and deuterium elimination pathways, respectively. However, since no hydrogen elimination was observed, we can conclude that the reaction does not proceed *via* intermediate **t8**. This can be readily understood in terms of the underlying triplet potential energy surface. Here, the formation of **t8** requires the rearrangement of **t3** *via* a barrier located about 137 kJ mol⁻¹ above **t3**. On the other hand, a second pathway to form the partially deuterated isotopomer of the penta-2,4-diynyl-1 radical [C₅H₃(X²B₁),

HCCCCCH₂], *i.e.* d2-penta-2,4-diynyl-1 [C₅D₂H, HCCCCD₂], can proceed *via* the reaction (**t3** → **t2** → **t1** → **t4** → **t5** → **t6** → **t7**). In this reaction sequence, the critical, rate-determining transition state for the **t4** → **t5** isomerization has a similar energy, −58.2 kJ mol^{−1} relative to the initial reactants, as the transition state for the **t3** → **t8** rearrangement, −56.7 kJ mol^{−1}. However, the transition state between **t4** and **t5** is much looser than that between **t3** and **t8**; the three lowest calculated real vibrational frequencies for the former are 76, 156, and 204 cm^{−1} as compared to 316, 388, and 408 cm^{−1} for the latter. This makes the number of vibrational states for TS **t4–t5** significantly higher than that for TS **t3–t8** at similar available internal energies. As a result, the overall rate constant for the **t3** → **t2** → **t1** → **t4** → **t5** → **t6** → **t7** isomerization sequence should be significantly higher than the rate constant for the **t3** → **t8** rearrangement. The decomposition of **t7** to the d2-penta-2,4-diynyl-1 [C₅HD₂, HCCCCD₂] can account for the observed deuterium loss pathway. Summarized, on the triplet surface of the dicarbon with methylacetylene reaction, the penta-2,4-diynyl-1 [C₅H₃(X²B₁), HCCCCCH₂] plus atomic hydrogen pathway presents the only observable channel. Similar to the dicarbon–acetylene reaction on the triplet surface, the dicarbon molecule does not separate in the ring opening process and yields a HCCCCCH₂ structure in which the dicarbon molecule is formally inserted between both (former) acetylenic carbon atoms. The relatively shallow potential energy wells might account for backward-scattered center-of-mass angular distributions and hence a shorter lifetime of the fragmenting **t7** complex. On the singlet surface, however, the understanding to what extent **s4** and **s5**—either of these intermediates is required to form the penta-1,4-diynyl-3 radical [C₅H₃(X²B₁), HCCCCHCCH]—is involved, is currently in progress. Note, that the isomerization of **s2** to **s3** involves a transition state similar to the reaction of singlet dicarbon with acetylene, and the carbon atoms of the reacting dicarbon molecule formally split up to yield a distinct penta-2,4-diynyl-1 radical [C₅H₃(X²B₁), HCCCCCH₂] (Fig. 14 and 16).

6.5. The dicarbon [C₂(X¹Σ_g⁺/a³Π_u)]-allene [H₂CCCH₂(X¹A₁)] system

Similar to the dicarbon plus methylacetylene reaction, both the penta-2,4-diynyl-1 [C₅H₃(X²B₁), HCCCCCH₂] and/or the penta-1,4-diynyl-3 [C₅H₃(X²B₁) HCCCCHCCH] can account for the experimentally determined reaction exoergicity (Table 3, Fig. 15). Therefore, we have to combine our experimental results with the computed potential energy surfaces to resolve this question. The center-of-mass angular distributions suggest indirect scattering dynamics and hence the existence of C₅H₄ intermediate(s). On the singlet surface, the decomposition of pentatetraene **s2** formed *via* isomerization of a cyclic intermediate **s1**. On the singlet surface, **s2** can fragment to form the penta-2,4-diynyl-1 radical [C₅H₃(X²B₁), HCCCCCH₂]; note that the penta-1,4-diynyl-3 radical [C₅H₃(X²B₁) HCCCCHCCH] cannot be synthesized on the singlet surface; isomerizations involving H migrations in **s2** are expected to be slower than the H loss. On the other hand, the triplet surface can support the generation of the less stable penta-1,4-diynyl-3 radical as well as the energetically favorable penta-2,4-diynyl-1 isomer *via* decomposing triplet intermediates **t5** and **t6**, respectively. We can now have a detailed look at the center-of-mass angular distributions to resolve which of these intermediates plays a major role in the underlying dynamics. The singlet and triplet

Table 3 Experimentally determined (Δ_rG(exp)) and computed reaction energies (Δ_rG(comp)) to form various hydrocarbon radicals in the reactions of dicarbon with acetylene, ethylene, methylacetylene, and allene. The computed energy difference between the triplet and singlet surface of about 9 kJ mol^{−1} is in excellent agreement with the experimental splitting of 8.6 kJ mol^{−1}

Reactant	Δ _r G (exp)/ kJ mol ^{−1}	Δ _r G (comp; singlet)/ kJ mol ^{−1}	Δ _r G (comp; triplet)/ kJ mol ^{−1}	Product isomer
Acetylene	40 ± 5	33 ± 5	42 ± 5	HCCCC
Ethylene	175 ± 10	156 ± 5	165 ± 5	H ₂ CCCCH
Methylacetylene	181 ± 12	192 ± 5	201 ± 5	H ₂ CCCCCH
		191 ± 5	200 ± 5	HCCCCHCCH
Allene	191 ± 11	195 ± 5	204 ± 5	H ₂ CCCCCH
		—	202 ± 5	HCCCCHCCH

pentatetraene intermediates **s2** and **t5** have C_2 rotational axes parallel to their principal rotational axes. Therefore, a hydrogen emission from **s2** and **t5** is expected to result in forward-backward symmetric center-of-mass angular distributions. However, the involvement of **t6** which is formed *via* a hydrogen shift from the initial collision complex **t1** might account for the backward scattered distributions observed experimentally. Here, **t6** belongs to the C_s point group and hence holds no C_2 rotational axis. Therefore, the involvement of a decomposing intermediate **t6** can account for the asymmetry at higher collision energies in the angular distributions and hence the formation of the penta-1,4-diynyl-3 radical [$C_5H_3(X^2B_1)$ HCCCCHCH] on the triplet surface. Summarized, the following reaction dynamics can be proposed. The dicarbon molecule—recall that we have dicarbon in its $X^1\Sigma_g^+$ electronic ground state as well as in its first electronically excited $a^3\Pi_u$ state—adds to the carbon-carbon double bond of the allene molecule forming the **s1** collision complex on the singlet surface. The latter isomerizes to **s2** which fragments *via* an atomic hydrogen loss to the penta-2,4-diynyl-1 radical [$C_5H_3(X^2B_1)$, HCCCCCH₂]. On the triplet surface, dicarbon can also add to the carbon-carbon double bond to form **t1** and **t7**. Both initial collision complexes rearrange to yield eventually **t5** and **t6**, respectively, which decompose to two distinct C_5H_3 radicals. The exit transition states deserve particular attention and can be better understood if we look at how the wave function changes in the course of the reverse reactions. In HCCCCHCH (X^2B_1), the unpaired electron is located at a molecular orbital (MO) perpendicular to the plane of molecule and antisymmetric with respect to this plane. When the hydrogen atom adds to this structure to form **t7** ($^3A'$) on the triplet surface, two single electrons are pushed to two a' -symmetric MOs lying in the molecular plane and one of two triple C≡C bonds in the reacting C_5H_3 radical becomes a double bond in the product. Thus, the rearrangement of electronic structure during the reaction is very significant and the process involves a high barrier of 133 kJ mol^{-1} . On the other hand, when a hydrogen atom adds to HCCCCCH₂ (X^2B_1) to form **t5** (3A_u), during the reaction course one unpaired electron remains at an orbital perpendicular to the molecular plane and the second remains at MO lying in this plane. Essentially, no CC bonds are broken, the rearrangement of the electronic structure is not so significant and only a low barrier, if any, can be expected. The calculations at the B3LYP level gave a late, product-like, but distinct transition state for the H loss from **t5** with a small barrier, however, at the G2M level the energy of this TS is 1 kJ mol^{-1} lower than that of the products. Within error bars of the present calculations, the exit barrier if it exists should not be higher than $5\text{--}10 \text{ kJ mol}^{-1}$.

7. Astrophysical implications

The carbon star IRC + 10216 is the brightest carbon rich object in the infrared sky.⁴⁸ It has an extended envelope in which more than 60 species have been observed. This object is particularly carbon rich, as many carbon clusters C_n ($n = 2, 3, 5$), hydrogen deficient carbon chains C_nH ($n = 2\text{--}8$), cyanopolyynes (HC_{2n}CN ($n = 1\text{--}4$)), their radicals $C_{2n}CN$ ($n = 1\text{--}2$), cummulenes C_nH_2 ($n = 3, 4, 6$), and hydrocarbons (CH₄, C₂H₂, C₂H₄, ¹³CH₃CCH) have been identified in its circumstellar envelope.⁴⁹ Note, that the isomer of methylacetylene, allene, has not been observed explicitly in the circumstellar envelope. However, the chemical reaction networks predict that the allene isomer should be present in the shell of IRC + 10216 as well.⁵⁰ The detection of methane, acetylene, ethylene, together with the silane molecule (SiH₄) makes this object especially valuable since these molecules have no permanent dipole moment and hence are not detectable with radio spectroscopy; therefore powerful infrared (IR) background sources and cutting-edge telescopes such as the NASA Infrared Telescope Facility (IRTF) on Mauna Kea are crucial. IRC + 10216 depicts an unprecedented variety of metal bearing species like NaCl, AlCl, AlF, KCl, NaCN, AlNC, MgCN, and MgNC, whose vibrational temperatures have been determined to be $700\text{--}1500 \text{ K}$. With the exception of SiC₂, SiC₃, and SiC₄ as well as the metal-bearing species, all molecules in the circumstellar envelope have been observed in interstellar clouds. Note, that unsaturated hydrocarbons have also been detected in cold molecular clouds such as OMC-1 and TMC-1. Here, methylacetylene has been detected in high fractional abundances between $4\text{--}6 \times 10^{-9} \text{ cm}^{-3}$ *via* microwave spectroscopy.⁵¹ The second isomer, allene, holds no permanent electric dipole moment and hence remains—in a similar manner to acetylene, ethylene, and dicarbon—unobservable *via* radio telescopes. However, despite these limitations, chemical reaction models predict that allene, ethylene, acetylene, and dicarbon are expected to be present in dark, molecular clouds, too.⁵² These

considerations make it exceptionally clear that the carbon star IRC + 10216 resembles a natural reservoir of both the dicarbon and acetylene, ethylene, methylacetylene, and allene reactant molecules.

In our studies, we identified four hydrocarbon radical products in the reactions of acetylene (R1), ethylene (R2), allene (R3), and methylacetylene (R4) with dicarbon (Fig. 11). These are buta-1,3-diynyl [$C_4H(X^2\Sigma^+)$, HCCCC (R1)], 1-butene-3-yne-2-yl [$i-C_4H_3(X^2A')$, H_2CCCCH (R2)], penta-2,4-diynyl-1 [$C_5H_3(X^2B_1)$, HCCCCCH₂ (R3, R4)], and penta-1,4-diynyl-3 radical [$C_5H_3(X^2B_1)$, HCCCCHCCH (R3, R4)] (Fig. 12–16). These results have strong astrophysical implications.

First, our findings can help to explain the formation of the linear buta-1,3-diynyl radical ($C_4H(X^2\Sigma^+)$) as detected towards cold molecular clouds (TMC-1, OMC-1) and the carbon star IRC + 10216. To the best of our knowledge, no ion–molecule reaction network can explain the formation of this radical quantitatively. Therefore, the crossed beams data present compelling evidence that barrier-less and exoergic neutral–neutral reactions might produce the buta-1,3-diynyl radical under single collision conditions *via* reactions of dicarbon in its $X^1\Sigma_g^+$ electronic ground state with acetylene.

Secondly, the crossed beams and theoretical studies predict the existence of three hitherto undetected interstellar hydrogen-deficient radicals: 1-butene-3-yne-2-yl [$i-C_4H_3(X^2A')$ H_2CCCCH] and the structural isomers penta-2,4-diynyl-1 [$C_5H_3(X^2B_1)$, HCCCCCH₂] and penta-1,4-diynyl-3 [$C_5H_3(X^2B_1)$ HCCCCHCCH]. Since both the dicarbon and the hydrocarbon reactants have been either observed or predicted by astrochemical models in the circumstellar envelope of IRC + 10216 and in the Orion and Taurus Molecular Clouds, our examinations can therefore guide future astronomical searches for these radicals. Actually, the situation of the 1-butene-3-yne-2-yl radical [$i-C_4H_3(X^2A')$ H_2CCCCH] is pretty interesting. In its ground state, this radical is bent and belongs to the C_s point group (all atoms are in the mirror plane). The butatrienyl structure, in which the carbon atoms are arranged in a linear structure, defines a C_{2v} symmetric transition state between two bent states, located only 255 cm^{-1} (366 K ; 3 kJ mol^{-1}) above the $i-C_4H_3$ structure. Since the coldest molecular clouds have averaged translational temperatures of about 10 K —about 7 cm^{-1} — $i-C_4H_3$ is bent in these environments since the transition state is energetically not accessible. However, in warmer (inner) regions of circumstellar envelopes, the inherent barrier could be overcome, and $i-C_4H_3$ radicals should be quasi linear. Consequently, the microwave spectrum of the $i-C_4H_3$ radical depends strongly on the temperature of the interstellar environment. *Vice versa*, recording these microwave spectra could serve as a probe to sample the temperature in distinct regions of the circumstellar envelope.

Thirdly, all radicals are expected to play a significant role in formation of aromatic ring(s) in extraterrestrial environments. The penta-2,4-diynyl-1 radical represents also an important resonance-stabilized free radical (RSFRs),¹ compared to the propargyl radical [$HCCCCH_2(X^2B_1)$]¹—thought to be a major growth species to form the very first aromatic ring in oxygen-poor and hydrocarbon rich environments—the penta-2,4-diynyl-1 radical is expanded by one carbon–carbon triple bond to give rise to a linear heavy carbon atom backbone and its reaction with the methyl radical may efficiently produce benzene or phenyl radical plus atomic hydrogen.^{53,54} Therefore, the inclusion of the reaction products of these neutral–neutral reactions into astrochemical models of carbon rich circumstellar envelopes and molecular clouds will lead to a refined understanding on the formation of polycyclic aromatic hydrocarbons (PAHs), their hydrogen deficient precursors, and of carbon-rich nanostructures.

Fourthly, we would like to address the involvement of the first electronically excited $a^3\Pi_u$ state of the dicarbon molecule. In cold molecular clouds and in the low temperature outer circumstellar envelopes of carbon stars, dicarbon molecules exist solely in their electronic ground state. Therefore, reactions of $C_2(a^3\Pi_u)$ are not relevant in these interstellar environments. However, close to the photosphere of the carbon stars, the strong photon field can photodissociate acetylene molecules *via* ethynyl radicals $C_2H(X^2\Sigma^+)$ to yield eventually dicarbon molecules in their electronic ground and in various electronically excited states.⁵⁵ These processes are similar to the two-photon dissociation of the ethynyl radical in cometary comae.⁵⁶ Therefore, reactions of dicarbon molecules in their $a^3\Pi_u$ state with unsaturated hydrocarbons may also become important in cometary comae and in regions of circumstellar envelopes close to the central star.

Finally, although this *Faraday Discussion* paper focuses on the reactions of dicarbon molecules in circumstellar envelopes and cold molecular clouds, these examinations also hold strong ties to

combustion processes in oxygen-poor hydrocarbon flames.¹ Here, astrophysicists and combustion chemists have utilized comparable reaction networks to model the chemistry of interstellar and flame environments; multi-component models of carbon cluster growth and the correlation with PAHs and soot formation are typical cases involving highly reactive carbon chains and hydrogen-deficient hydrocarbon radicals such as buta-1,3-diyne-1-yl [$C_4H(X^2\Sigma^+)HCCCC$] and most importantly the 1-butene-3-yne-2-yl radical [$i-C_4H_3(X^2A')H_2CCCCH$].^{57,58} Therefore, our findings can also help to shed light on explaining the formation of these radicals in oxygen-poor combustion flames. Most important, in denser environments like combustion processes, the internally excited intermediates of the reactions of dicarbon with the hydrocarbon molecules can be stabilized *via* a third body reaction. This effectively diverts (a fraction of) the excess energy from the intermediates to the third body thus stabilizing the intermediates involved. Note, that these processes are not important in cold molecular clouds and in the outer regions of the circumstellar envelopes where solely bimolecular reactions prevail. Therefore, the chemistry of hydrocarbon flames is clearly more complicated; future chemical models of oxygen-poor combustion flames should therefore also incorporate the reaction intermediates involved in the present studies to yield a complete picture on the formation of hydrogen-poor carbonaceous molecules in these environments.

8. Conclusions

Our investigations demonstrated that the bimolecular reactions of dicarbon molecules with acetylene, ethylene, methylacetylene, and allene proceed without an entrance barrier and through indirect (complex forming) scattering dynamics. Each reaction is initiated by an addition of the dicarbon molecule to the π bond of the unsaturated hydrocarbon molecule yielding initially acyclic (triplet surface) as well as three- and four-membered cyclic collision complexes (triplet and singlet surfaces). On the singlet surface, the cyclic structures isomerize to form eventually diacetylene ($HCCCCH$; C_2/C_2H_2), butatriene (H_2CCCCH_2 ; C_2/C_2H_4), methylacetylene (CH_3CCCCH ; C_2/CH_3CCH), and pentatetraene ($H_2CCCCCH_2$; C_2/H_2CCCH_2) intermediates. The latter were found to decompose barrierless *via* atomic hydrogen loss yielding buta-1,3-diyne-1-yl [$C_4H(X^2\Sigma^+)HCCCC$], 1-butene-3-yne-2-yl [$i-C_4H_3(X^2A')H_2CCCCH$], penta-2,4-diyne-1 [$C_5H_3(X^2B_1)HCCCCCH_2$], and penta-1,4-diyne-3 radical [$C_5H_3(X^2B_1)HCCCHCCH$] under single collision conditions; both the experiments and RRKM calculations agree that molecular hydrogen loss pathways are unimportant and contribute less than 1% to the scattering signal. The overall reactions to form the hydrogen-deficient radicals were found to be exoergic. The underlying characteristics (indirect scattering dynamics; no entrance barrier; isomerization barriers below the energy of the separated reactants; exoergic reactions) suggests the enormous potential of the dicarbon plus unsaturated hydrocarbon reaction class to form highly hydrogen-deficient carbonaceous molecules in cold molecular clouds and in circumstellar envelopes of carbon stars. In denser environments such as in comets and related oxygen-poor combustion flames, the identified reaction intermediates can also be stabilized *via* a third body collision. We would like to mention that our collision energies are actually higher than the equivalent temperature in cold molecular clouds. However, in the case of the dicarbon plus acetylene, ethylene, and allene, we observed only one reaction product, *i.e.* the buta-1,3-diyne-1-yl [$C_4H(X^2\Sigma^+)HCCCC$] and 1-butene-3-yne-2-yl [$i-C_4H_3(X^2A')H_2CCCCH$], and the penta-2,4-diyne-1 radical [$C_5H_3(X^2B_1)HCCCCCH_2$], respectively, on the singlet surface. Therefore, based on our investigations, even at lower collision energies, only one isomer is formed on the singlet surface. On the other hand, the involvement of two isomers in the dicarbon–methylacetylene reaction and their branching ratio could be sensitive to the collision energy and hence temperatures. This is currently under investigation. Summarized, our studies present an important advancement to establish a comprehensive database of reaction intermediates and products involved in bimolecular collisions of dicarbon molecules with unsaturated hydrocarbons which can be utilized in refined astrochemical models and also in future searches of hitherto unidentified interstellar molecules.

Acknowledgements

The experimental and theoretical work was supported by the US Department of Energy-Basic Energy Sciences (DE-FG02-03ER15411 and DE-FG02-04ER15570); the construction of the crossed beams machine was also aided by the National Science Foundation (CHE-0234461).

References

- 1 Jürgen Wolfrum, *Faraday Discuss.*, 2001, **119**, 1.
- 2 (a) R. D. Kern *et al.*, *Combust. Sci.*, 1992, **85**, 77; (b) J. H. Kiefer *et al.*, *Combust. Sci. Technol.*, 1992, **82**, 101; (c) C. E. Baukal, *Oxygen-enhanced combustion*, CRS Press, New York, 1998.
- 3 (a) Y. C. Minh and E. F. Dishoeck, *Astrochemistry – From Molecular Clouds to Planetary Systems*, ASP Publisher, San Francisco, 2000; (b) David A. Williams, *Faraday Discuss.*, 1998, **109**, 1; (c) H. J. Fraser *et al.*, *Astron. Geophys.*, 2002, **43**, 10; (d) R. I. Kaiser, C. Ochsenfeld, D. Stranges, M. Head-Gordon and Y. T. Lee, *Faraday Discuss.*, 1998, **109**, 183; (e) C. C. Chiong, O. Asvany, N. Balucani, Y. T. Lee and R. I. Kaiser, *Nucleation of hydrogen deficient carbon clusters in circumstellar envelopes of carbon stars*, World Scientific Press, Proceedings of the 8th Asia-Pacific Physics Conference, APPC 2000, 2001, p. 167; (f) R. I. Kaiser and N. Balucani, *Int. J. Astrobiol.*, 2002, **1**, 15.
- 4 (a) J. Appel, H. Bockhorn and M. Frenklach, *Combust. Flame*, 2000, **121**, 122; (b) A. Kazakov and M. Frenklach, *Combust. Flame*, 1998, **114**, 484; (c) A. Kazakov and M. Frenklach, *Combust. Flame*, 1998, **112**, 270; (d) L. Vereecken, H. F. Bettinger and J. Peeters, *Phys. Chem. Chem. Phys.*, 2002, **4**, 2019; (e) P. Ehrenfreund and S. B. Charnley, *Annu. Rev. Astron. Astrophys.*, 2000, **38**, 427; (f) H. Richter, Oleg A. Mazyar, Raman Sumathi, William H. Green, Jack B. Howard and Joseph W. Bozzelli, *J. Phys. Chem. A*, 2001, **105**, 1561.
- 5 (a) J. Appel, H. Bockhorn and M. Frenklach, *Combust. Flame*, 2000, **121**, 122; (b) H. Richter and J. B. Howard, *Prog. Energy Combust. Sci.*, 2000, **26**, 565; (c) C. Baird, *Environmental Chemistry*, W. H. Freeman Company, New York, 1999; (d) R. I. Kaiser, H. Y. Lee, A. M. Mebel and Y. T. Lee, *Astrophys. J.*, 2001, **548**, 852.
- 6 (a) B. E. Turner, *Astrophys. J.*, 2000, **542**, 837; (b) S. Viti, D. A. Williams and P. T. O'Neill, *Astron. Astrophys.*, 2000, **354**, 1062.
- 7 M. Lindqvist *et al.*, *Astron. Astrophys.*, 2000, **361**, 1036.
- 8 R. I. Kaiser, *Chem. Rev.*, 2002, **102**, 1309.
- 9 (a) J. M. Hollis *et al.*, *Astrophys. J.*, 2001, **554**, 181; (b) J. M. Hollis *et al.*, *Astrophys. J.*, 2000, **540**, 1107; (c) G. Horneck and C. Baumstark-Khan, ed. *Astrobiology*, Springer, Berlin, 2002.
- 10 D. A. Williams and T. W. Hartquist, *Acc. Chem. Res.*, 1999, **32**, 334.
- 11 (a) A. Brack, *The Molecular Origins of Life—Assembling Pieces of the Puzzle*, Cambridge University Press, Cambridge, 1998. ESA Special Publication SP-496, *Exo- and Astrobiology*, 2001; (b) A. Richards and P. Sarre, *Astron. Geophys.*, 2001, **6**, 17; (c) E. Bergin, *Chem. Ind.*, 2001, **8**, 659.
- 12 (a) O. Guillois, G. Ledoux and C. Reynaud, *Astrophys. J. Lett.*, 1999, **521**, 133; (b) P. John *et al.*, *Diamond Relat. Mater.*, 2002, **11**, 608.
- 13 (a) F. Battin-Leclerc, *Phys. Chem. Chem. Phys.*, 2002, **4**, 2072; (b) Katharina Kohse-Höinghaus, Burak Atakan, Axel Lamprecht, Guillermo González Alatorre, Michael Kamphus, Tina Kasper and Ning-Ning Liu, *Phys. Chem. Chem. Phys.*, 2002, **4**, 2056; (c) H. Richter and J. B. Howard, *Phys. Chem. Chem. Phys.*, 2002, **4**, 2038; (d) M. Frenklach, *Phys. Chem. Chem. Phys.*, 2002, **4**, 2028.
- 14 <http://www.cv.nrao.edu/~awooten/allmols.html>.
- 15 (a) T. J. Millar, E. Herbst and R. P. A. Bettens, *Mon. Not. R. Astron. Soc.*, 2000, **316**, 195; (b) R. P. A. Bettens and E. Herbst, *Astrophys. J.*, 1995, **443**, 664.
- 16 M. Dobrijevic and J. P. Parisot, *Planet. Space Sci.*, 1998, **46**, 491.
- 17 <http://www.aas.org/~dps/decadal/>.
- 18 (a) W. M. Pitts, L. Pasternack and J. R. McDonald, *Chem. Phys.*, 1982, **68**, 417; (b) L. Pasternack, W. M. Pitts and J. R. McDonald, *Chem. Phys.*, 1981, **57**, 19; (c) V. M. Donnelly and L. Pasternack, *Chem. Phys.*, 1979, **39**, 427; (d) L. Pasternack and J. R. McDonald, *Chem. Phys.*, 1979, **43**, 173; (e) H. Reisler, M. Mangir and C. Wittig, *J. Chem. Phys.*, 1979, **71**, 2109; (f) K. H. Becker, B. Donner, H. Geiger, F. Schmidt and P. Wiesen, *Z. Phys. Chem.*, 2000, **214**, 503; (g) M. Martin, *J. Photochem. Photobiol., A*, 1992, **A66**, 263.
- 19 P. S. Skell, L. M. Jackman, S. Ahmed, M. L. McKee and P. B. Shevlin, *J. Am. Chem. Soc.*, 1989, **111**, 4422.
- 20 S. B. Yorke, *Astrophys. J.*, 1983, **88**, 1816.
- 21 I. A. Crawford and M. J. Barlow, *Mon. Not. R. Astron. Soc.*, 2000, **311**, 370.
- 22 (a) P. Casavecchia, *Rep. Prog. Phys.*, 2000, **63**, 355; (b) P. Casavecchia, N. Balucani and G. Volpi, *Annu. Rev. Phys. Chem.*, 1999, **50**, 347.
- 23 X. Gu, Y. Guo, A. M. Mebel and R. I. Kaiser, *J. Phys. Chem. A*, 2006, submitted.
- 24 Y. Guo, X. Gu, E. Kawamura and R. I. Kaiser, *Rev. Sci. Instrum.*, 2005, submitted.
- 25 R. I. Kaiser, C. Ochsenfeld, D. Stranges, M. Head-Gordon and Y. T. Lee, *Faraday Discuss.*, 2001, **119**, 183.
- 26 R. I. Kaiser and A. M. Mebel, *Int. Rev. Phys. Chem.*, 2002, **21**, 307.
- 27 (a) R. I. Kaiser, J. W. Ting, L. C. L. Huang, N. Balucani, O. Asvany, Y. T. Lee, H. Chan, D. Stranges and D. Gee, *Rev. Sci. Instrum.*, 1999, **70**, 4185; (b) X. Gu, Y. Guo, H. Chan, E. Kawamura and R. I. Kaiser, *Rev. Sci. Instrum.*, 2005, in press.
- 28 G. O. Brink, *Rev. Sci. Instrum.*, 1996, **37**, 857.
- 29 (a) N. R. Daly, *Rev. Sci. Instrum.*, 1960, **31**, 264; (b) X. Gu, Y. Guo, E. Kawamura and R. I. Kaiser, *Rev. Sci. Instrum.*, 2005, in press.
- 30 X. Gu, Y. Guo, E. Kawamura and R. I. Kaiser, *Rev. Sci. Instrum.*, 2005, **76**, 083115-1-6.

- 31 R. I. Kaiser, C. Ochsenfeld, D. Stranges, M. Head-Gordon and Y. T. Lee, *Faraday Discuss.*, 1998, **109**, 183.
- 32 (a) M. S. Weiss, PhD Thesis, 1986, University of California, Berkeley; (b) M. Vernon, PhD Thesis, 1981, University of California, Berkeley.
- 33 X. Gu, Y. Guo and R. I. Kaiser, *Int. J. Mass Spectrom.*, 2005, **246**, 29.
- 34 A. M. Mebel, K. Morokuma and M. C. Lin, *J. Chem. Phys.*, 1995, **103**, 7414.
- 35 (a) G. D. Purvis and R. J. Bartlett, *J. Chem. Phys.*, 1982, **76**, 1910; (b) C. Hampel, K. A. Peterson and H. J. Werner, *Chem. Phys. Lett.*, 1992, **190**, 1; (c) P. J. Knowles, C. Hampel and H. J. Werner, *J. Chem. Phys.*, 1994, **99**, 5219; (d) M. J. O. Deegan and P. J. Knowles, *Chem. Phys. Lett.*, 1994, **227**, 321.
- 36 A. D. Becke, *J. Chem. Phys.*, 1993, **98**, 5648.
- 37 C. Lee, W. Yang and R. G. Parr, *Phys. Rev. B*, 1988, **37**, 785.
- 38 M. J. Frisch, G. W. Trucks, H. B. Schlegel, G. E. Scuseria, M. A. Robb, J. R. Cheeseman, V. G. Zakrzewski, J. A. Montgomery Jr, R. E. Stratmann, J. C. Burant, S. Dapprich, J. M. Millam, A. D. Daniels, K. N. Kudin, M. C. Strain, O. Farkas, J. Tomasi, V. Barone, M. Cossi, R. Cammi, B. Mennucci, C. Pomelli, C. Adamo, S. Clifford, J. Ochterski, G. A. Petersson, P. Y. Ayala, Q. Cui, K. Morokuma, D. C. Malick, A. D. Rabuck, K. Raghavachari, J. B. Foresman, J. Cioslowski, J. V. Ortiz, A. G. Baboul, B. B. Stefanov, G. Liu, A. Liashenko, P. Piskorz, I. Komaromi, R. Gomperts, R. L. Martin, D. J. Fox, T. Keith, M. A. Al-Laham, C. Y. Peng, A. Nanayakkara, C. Gonzalez, M. Challacombe, P. M. W. Gill, B. Johnson, W. Chen, M. W. Wong, J. L. Andres, C. Gonzalez, M. Head-Gordon, E. S. Replogle and J. A. Pople, *GAUSSIAN 98 (Revision A.7)*, Gaussian, Inc., Pittsburgh PA, 1998.
- 39 *MOLPRO* is a package of *ab initio* programs written by H.-J. Werner and P. J. Knowles with contributions from J. Almlöf, R. D. Amos, M. J. O. Deegan, S. T. Elbert, C. Hampel, W. Meyer, K. Peterson, R. Pitzer, A. J. Stone, P. R. Taylor and R. Lindh.
- 40 (a) A. M. Mebel, V. V. Kislov and R. I. Kaiser, *J. Phys. Chem. A*, 2005, in press; (b) A. M. Mebel and R. I. Kaiser, in preparation.
- 41 N. Balucani, H. Y. Lee, A. Mebel, Y. T. Lee and R. I. Kaiser, *J. Chem. Phys.*, 2001, **115**, 5107.
- 42 R. I. Kaiser, A. M. Mebel, Y. T. Lee and A. H. H. Chang, *J. Chem. Phys.*, 2001, **115**, 5117.
- 43 R. I. Kaiser, O. Asvany, Y. T. Lee, H. F. Bettinger, P. v. R. Schleyer and H. F. Schaefer III, *J. Chem. Phys.*, 2000, **112**, 4994.
- 44 R. I. Kaiser, A. M. Mebel and Y. T. Lee, *J. Chem. Phys.*, 2001, **114**, 231.
- 45 R. I. Kaiser, T. L. Nguyen, A. M. Mebel and Y. T. Lee, *J. Chem. Phys.*, 2002, **116**, 1318.
- 46 R. I. Kaiser, C. Ochsenfeld, M. Head-Gordon, Y. T. Lee and A. G. Suits, *Science*, 1996, **274**, 1508.
- 47 R. I. Kaiser and A. M. Mebel, *Int. Rev. Phys. Chem.*, 2002, **21**, 307.
- 48 T. J. Millar, E. Herbst and R. P. A. Bettens, *Mon. Not. R. Astron. Soc.*, 2000, **316**, 195.
- 49 (a) G. M. Guélin, J. Cernicharo, M. J. Travers, M. C. McCarthy, C. A. Gottlieb, P. Thaddeus, M. Ohishi, S. Saito and S. Yamamoto, *Astron. Astrophys.*, 1997, **317**, L1; (b) C. Jose, Y. Iseai, G.-A. Eduardo, D. J. Teije, H. Ana, E. Rafael and O. Juan, *Astrophys. J.*, 1999, **526**, L41; (c) K. H. Hinkle and J. J. Keady, *Astrophys. J.*, 1988, **331**, 539; (d) A. L. Betz, *Astrophys. J.*, 1981, **244**, L103; (e) D. M. Goldhaber, A. L. Betz and J. J. Ottusch, *Astrophys. J.*, 1987, **314**, 356.
- 50 J. M. Brown and T. J. Millar, *Mon. Not. R. Astron. Soc.*, 2003, **339**, 1041.
- 51 (a) E. C. Sutton, R. Peng, W. C. Danchi, P. A. Jaminet, G. Sandell and A. P. G. Russel, *Astrophys. J., Suppl. Ser.*, 1995, **97**, 455; (b) F. Combes, G. Wlodarczak, P. Encrenaz and C. Laurent, *Astron. Astrophys.*, 1992, **253**, L29.
- 52 (a) T. J. Millar, P. R. A. Farquhar and K. Willacy, *Astron. Astrophys., Suppl. Ser.*, 1997, **121**, 139; (b) A. J. Markwick, T. J. Millar and S. B. Charnley, *Astrophys. J.*, 2000, **535**, 256; (c) P. Pratap, J. E. Dickens, R. L. Snell, M. P. Miralles, E. A. Bergin, W. M. Irvine and F. P. Schloerb, *Astrophys. J.*, 1997, **486**, 862.
- 53 V. V. Kislov, T. L. Nguyen, A. M. Mebel, S. H. Lin and S. C. Smith, *J. Chem. Phys.*, 2004, **120**, 7008.
- 54 J. A. Miller, *Faraday Discuss.*, 2001, **119**, 461.
- 55 (a) A. Fuente, J. Cernicharo and A. Omont, *Astron. Astrophys.*, 1998, **330**, 232; (b) I. Cherchneff and A. E. Glassgold, *Astrophys. J.*, 1993, **419**, L41; (c) K. H. Hinkle and J. J. Keady, *Astrophys. J.*, 1988, **331**, 539; (d) P. J. Huggins, W. J. Carlson and A. L. Kinney, *Astron. Astrophys.*, 1984, **133**, 347.
- 56 A. M. Mebel, M. Hayashi, W. M. Jackson, J. Wrobel, M. Green, D. Xu and S. H. Lin, *J. Chem. Phys.*, 2001, **114**, 9821.
- 57 G. Pascoli and A. Polleux, *Astron. Astrophys.*, 2000, **359**, 799.
- 58 (a) M. Ohishi and N. Kaifu, *Faraday Discuss.*, 1998, **109**, 205; (b) M. Guelin, S. Green and P. Thaddeus, *Astrophys. J.*, 1978, **224**, L27; (c) M. Cernicharo, C. Kahane, J. Gomez-Gonzalez and M. Guelin, *Astron. Astrophys.*, 1986, **164**, L1; (d) C. M. Walmsley, P. R. Jewell, L. E. Snyder and G. Winnewisser, *Astron. Astrophys.*, 1984, **134**, L11; (e) J. Cernicharo, M. Guelin, K. M. Menten and C. M. Walmsley, *Astron. Astrophys.*, 1987, **181**, L1; (f) J. Guelin *et al.*, *Astron. Astrophys.*, 1997, **317**, L1; (g) J. Cernicharo and M. Guelin, *Astron. Astrophys.*, 1996, **309**, L27; (h) C. A. Gottlieb, M. C. McCarthy, M. J. Travers and P. J. Thaddeus, *Chem. Phys.*, 1998, **109**, 5433; (i) T. J. Millar and E. Herbst, *Astron. Astrophys.*, 1994, **288**, 561.